HHS Public Access

Author manuscript

Cell Stem Cell. Author manuscript; available in PMC 2018 October 05.

Published in final edited form as:

Cell Stem Cell. 2017 October 05; 21(4): 502–516.e9. doi:10.1016/j.stem.2017.08.018.

MYC CONTROLS HUMAN PLURIPOTENT STEM CELL FATE DECISIONS THROUGH REGULATION OF METABOLIC FLUX

Timothy S. Cliff[1,2], **Tianming Wu**[1,2], **Benjamin R. Boward**[1,2], **Amelia Yin**[1,2], **Hang Yin**[1,2], **John N. Glushka**[1,3], **James H. Prestegaard**[1,3], and **Stephen Dalton**[1,2,*]

[1]Department of Biochemistry and Molecular Biology, University of Georgia, 500 D.W. Brooks Drive, Athens, GA 30602, USA

[2]Center for Molecular Medicine, University of Georgia, 500 D.W. Brooks Drive, Athens, GA 30602, USA

[3]Complex Carbohydrate Research Center, University of Georgia, 315 Riverbend Road, Athens, GA 30602, USA

SUMMARY

As human pluripotent stem cells (hPSCs) exit pluripotency they are thought to switch from a glycolytic mode of energy generation to one more dependent on oxidative phosphorylation. Here we show that although metabolic switching occurs during early mesoderm and endoderm differentiation, high glycolytic flux is maintained and in fact essential during early ectoderm specification. The elevated glycolysis observed in hPSCs requires elevated MYC/MYCN activity. Metabolic switching during endodermal and mesodermal differentiations coincides with a reduction in MYC/MYCN, and can be reversed by ectopically restoring MYC activity. During early ectodermal differentiation, sustained MYCN activity maintains the transcription of 'switch' genes that are rate-limiting for metabolic activity and lineage commitment. Our work, therefore, shows that metabolic switching is lineage-specific and not a required step for exit of pluripotency in hPSCs, and identifies MYC and MYCN as developmental regulators that couple metabolism to pluripotency and cell fate determination.

eTOC summary

*Correspondence and Lead Contact: sdalton@uga.edu.

AUTHOR CONTRIBUTIONS

TSC performed metabolic flux analysis, functional assays, cell culture, designed experiments and manuscript preparation; TW performed RNA-seq analysis; BRB performed flow cytometry experiments; AY and HY performed ECAR and OCR analysis with TSC; JNG and JHP established NMR workflow; SD designed experiments and manuscript preparation.

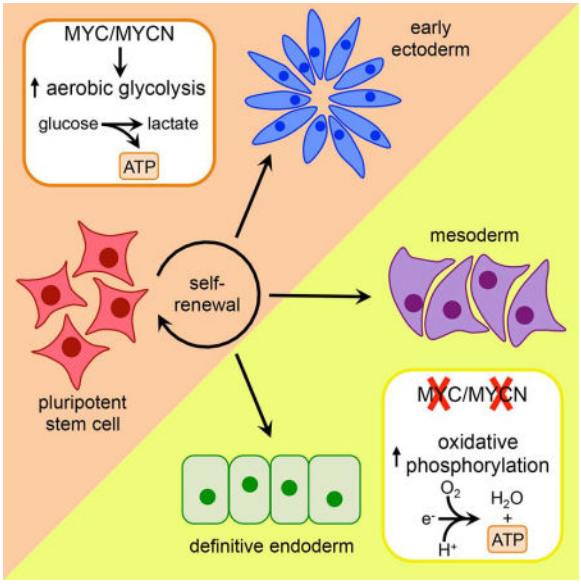

Dalton and colleagues show that, contrary to prior understanding, a metabolic switch away from glycolysis is not a required step for human pluripotent stem cell differentiation, and in fact differentiation to ectoderm requires maintenance of high glycolytic flux via MYC/MYCN activity indicating its role as a developmental regulator.

INTRODUCTION

Human embryonic stem cells (hESCs) and human induced pluripotent stem cells (hiPSCs) are thought to generate most of their energy by oxidation of glucose through the glycolytic pathway, consequently producing high levels of secreted lactate (Ryall et al., 2015a; Shyh-Chang and Daley, 2015). Unlike most cells grown under aerobic conditions, human pluripotent stem cells (hPSCs) do not rely heavily on oxidative phosphorylation (OxPhos) for ATP generation but instead utilize aerobic glycolysis (Varum et al., 2011; Zhang et al., 2011; Zhou et al., 2012), similar to that described for tumor cells (Vander Heiden et al., 2009). It is generally assumed that when hESCs and hiPSCs exit pluripotency, they undergo metabolic remodeling so that energy generation switches to a mechanism that is heavily dependent on OxPhos and less reliant on glycolysis (Gu et al., 2016; Moussaieff et al., 2015b; Varum et al., 2011; Zhang et al., 2011). This “metabolic switch” marked by a shift in dependency of glycolysis to OxPhos is based on studies where glycolytic rates for hPSCs are compared with fully-differentiated somatic cell lines, with only limited analysis of events following exit from pluripotency and commitment to the embryonic germ layers.

The question of whether elevated aerobic glycolysis is required for maintenance of pluripotency has been addressed by two groups (Gu et al., 2016; Moussaieff et al., 2015b). In these studies, inhibition of glycolysis was shown to promote spontaneous differentiation (Gu et al., 2016; Moussaieff et al., 2015b), consistent with it being required for maintenance of pluripotency. Besides having a role in energy generation, glycolytic flux in hPSCs generates elevated levels of acetate and acetyl CoA which contribute to an epigenetic landscape required for maintenance of pluripotency (Moussaieff et al., 2015b). This

observation provides a rationale to explain why hPSCs utilize aerobic glycolysis and is based on the concept that pluripotent cells have highly-acetylated, open chromatin in contrast to differentiated cells where it is more compacted. Establishment of aerobic glycolysis is also important for reprogramming of fibroblasts to the pluripotent state (Folmes et al., 2011; Kida et al., 2015). Findings in these reports have been interpreted to indicate that metabolic switching is causative for the establishment of pluripotency rather than being correlative. The mechanism by which metabolic switching occurs as hPSCs exit pluripotency is obscure and has not been addressed previously. Since metabolism is intimately linked to cell fate (Ryall et al., 2015a; Shyh-Chang and Daley, 2015), this reflects a large knowledge gap and highlights why it is critical to define the roles of these pathways in greater detail.

Using measurements of extracellular acidification rates (ECAR) and oxygen consumption rates (OCRs) as readouts for glycolysis and OxPhos, respectively, we find that although definitive endoderm (DE) and mesoderm (Meso) undergo metabolic switching following exit from pluripotency, nascent ectoderm retains elevated glycolytic flux. This was confirmed using heteronuclear single-quantum coherence (HSQC) nuclear magnetic resonance (NMR) spectroscopy of cells labeled with ^{13}C-glucose. Metabolic switching is therefore not a pre-requisite for pluripotency exit as previously proposed (Gu et al., 2016; Moussaieff et al., 2015b; Varum et al., 2011; Zhang et al., 2011) and only occurs in DE and Meso lineages. While investigating the mechanism of metabolic switching we found that transcriptional regulation of metabolic genes underpins the 'switch' during the early stages of pluripotent cell differentiation. This transcriptional program is orchestrated by the MYC transcription factor-family. In hPSCs, MYC and MYCN maintain transcription required for elevated glycolysis but both factors are lost during DE and Meso differentiation, resulting in metabolic switching. In ectoderm however, expression of MYCN is retained, allowing elevated glycolytic activity to be sustained. These findings indicate that MYC transcription factors serve as lineage-specific regulators of metabolic activity and serve as developmental regulators by coupling metabolic flux to cell fate decisions.

RESULTS

Metabolic switching as cells exit pluripotency is germ layer specific

The loss of aerobic glycolysis is believed to be an obligatory event during the differentiation of pluripotent stem cells (Gu et al., 2016; Moussaieff et al., 2015b; Varum et al., 2011; Zhang et al., 2011). This process, however, has only been evaluated in a limited number of differentiation models raising questions about the coupling between metabolism, pluripotency exit and transition towards the three embryonic germ layers. To address this we differentiated WA09 hESCs to DE, Meso and towards two nascent ectoderm progenitor cell types- neural progenitor cells (NPC) and early neural crest stem cells (NCSC) (Figure 1A). Primary human fibroblasts (Fibs) and their derivative iPSCs were included in the analysis as a source of fully differentiated and reprogrammed cells, respectively. Compared to Fibs, hPSCs (WA07, WA09 and hiPSCs) exhibited elevated ECARs after glucose stimulation (Figure 1B,C) consistent with them generating high levels of lactate. A high concentration of 2-deoxyglucose (2-DG; 50mM) was used to completely inhibit glycolysis and verify that

changes in ECAR measurements are due solely to glycolytic flux (Jan et al., 2016; Wang et al., 2017; Yang et al., 2017). Oligomycin had little impact on ECARs in hPSCs (Figure 1B) indicating that energy generation was largely independent of respiratory function and that hPSCs operate near their maximal glycolytic capacity (Figure 1C). Furthermore, Fibs showed higher rates of oligomycin-sensitive oxygen consumption, consistent with their greater dependency on OxPhos (Figure 1D,E). ECARs in DE and Meso showed only a minor response to glucose, indicative of low glycolytic rates (Figure 1C,F). Oligomycin increased ECARs in DE and Meso, as seen for Fibs (Figure 1C,F), indicating that glycolytic flux increases in response to respiratory inhibition. However, glycolytic capacity for DE, Meso and Fibs was less than that of hPSCs (Figure 1C,F). DE and Meso also show elevated rates of OxPhos relative to hPSCs and were comparable to Fibs (Figure 1D,G). These observations are consistent with DE and Meso having undergone metabolic switching. All ECAR and OCR measurements were made in the same growth factor-free media. Germ layer-specific differences in metabolic fluxes that we observe are therefore unlikely to be caused by culture conditions.

When ECARs for ectoderm cells were assayed, we were surprised to see that NPC and NCSC precursors retained elevated levels of glycolytic activity following exit from pluripotency (Figure 1C,F). Nascent ectoderm also displays near maximal glycolytic capacity (Figure 1C) and low levels of OxPhos (Figure 1E) as is also observed in hPSCs. These metabolic parameters indicate that metabolic switching does not occur as hPSCs transition to early ectoderm. Confirmation of hESC status and differentiation into the three germ layers is shown in Figure S1A,B. DE, Meso and NPC RNA-seq data from cells used in this study cluster with corresponding cell types generated by other laboratories (Bernstein et al., 2010; Chu et al., 2016; van de Leemput et al., 2014) by multidimensional scaling analysis. This indicates that cells being used here are comparable to others generated by the field. Doubling times of hESCs and their differentiated derivatives do not vary greatly (Figure S1D), although the percentage of G_0/G1 in early germ layer derivatives is increased relative to hESCs (Figure S1E). This indicates that differences in growth rates are not a major factor in determining differences in metabolic activity in PSCs and the three germ layers. Using ECARs and OCRs, we show that metabolic switching only occurs in DE and Meso following exit from pluripotency. In contrast, NPC and NCSC retain high glycolytic rates, elevated glycolytic capacity and low oxygen consumption rates. These observations raise questions about the general assumption that metabolic switching is an obligatory step for pluripotency exit.

Metabolic switching is germ layer specific as cells exit pluripotency

To confirm that DE and Meso, but not ectoderm, undergo metabolic switching following pluripotency exit we performed metabolic labeling with uniformly labeled ^{13}C-glucose followed by nuclear magnetic resonance (NMR)-based fluxome analysis. This approach provides a quantitative, temporal description of the metabolic landscape in pluripotency and the three hESC-derived germ layers. Because metabolic switching during early hESCs differentiation is associated with decreased glycolysis and lactate production, we focused on this pathway for ^{13}C-flux analysis. Cells were labeled over 0–4 hr with ^{13}C-glucose and H,C-HSQC NMR spectroscopy was performed on polar and non-polar fractions and media

for each cell type (Figure 2A). This time-course allowed us to directly track the fate of ^{13}C, the source of metabolites contributing to fluxomes and pathway utilization without the problems associated with longer periods of metabolic labeling. Representative spectra are shown in Figures 2B,C. After labeling with ^{13}C-glucose for different times, levels of ^{13}C-labeled metabolites were determined (Figure 2D) and displayed as a heat-map relative to levels in hESCs at equivalent time intervals (Figure 2E), highlighting the similar metabolic profile of NPCs to that of PSCs. This analysis includes quantitation of metabolites in the glycolytic pathway, hexosamine biosynthetic pathway, pentose phosphate pathway, tricarboxylic acid (TCA) cycle and generation of glutathione, acetate, glycogen and amino acids. As an example, lactate levels over a 4 hr ^{13}C-glucose labeling time-course are at least 50-fold higher for hPSCs and NPCs compared to Fibs and the two other hPSC-derived germ layers (Figure 2D). This analysis also identifies potential points of differential metabolic regulation between cell types. For example, hexokinase (HK) activity is saturated in DE and Meso as indicated by the accumulation of intracellular glucose relative to glucose 6-phosphate (Figure 2D). This is not observed in hPSCs and ectoderm indicating that HK activity is a potential point of metabolic regulation during development. This analysis indicates that rates of metabolite accumulation associated with glycolysis are high in hPSCs and ectoderm but significantly lower in Meso and DE. Lactate, acetate and alanine accumulation showed similar trends (Figure 2D). hESCs and ectoderm cells have a greater flux of carbon, in nmol/hr standardized to 25 million cells, for glycolytic intermediates, lactate, alanine, acetyl-CoA, and acetate (Figure S2A). This was determined by calculating the carbon flux for each metabolite over 4 hr. These data are consistent with ECAR analysis in Figure 1 showing that ectoderm does not undergo metabolic switching following exit from pluripotency. To determine when metabolic switching occurs in the ectoderm lineage, we evaluated the transition as NPCs transition to midbrain floor plate precursors as determined by the expression of *FOXA2* and *LMXA1* (Figure S2B) and loss of *PAX6* (Figure S2C) (Kirkeby et al., 2012; Kriks et al., 2011). Metabolic switching in the ectoderm lineage occurs after NPC identity is lost (d10) (Figure S2B–D), coinciding with the loss of *MYCN* and induction of *FOXA2*. This shows that ectoderm is capable of metabolic switching but that it is occurs under a different developmental time-line than DE and Meso.

Metabolites for the tricarbooxylic acid (TCA) cycle were also determined (Figure 2E). This analysis indicates that flux through the TCA cycle is elevated in Meso and DE relative to hPSCs and ectoderm. These data show that metabolic switching is clearly linked to specific cell fate transitions and not due to differences in differentiation rates along different lineages. Proliferation rates and cell cycle profiles for each germ layer are comparable (Figure S1D,E), ruling out the possibility that metabolic differences are due to cell division requirements. Overall, these observations raise important questions about the role of metabolic regulation in cell fate decisions (see Discussion).

These observations confirm that metabolic switching does not occur during early ectoderm germ layer formation following exit from pluripotency and only occurs in Meso and DE. In summary, metabolic switching is not an absolute requirement for exit from the pluripotent state, but is associated with specific cell fate decisions associated with the formation of Meso and DE.

Pluripotency and early ectoderm commitment requires elevated glycolytic flux

Results so far show that metabolic switching occurs in Meso and DE, but not nascent ectoderm, following pluripotency exit. We then asked if elevated aerobic glycolysis was important for maintenance of pluripotency and specification of early ectoderm. For these experiments, we used two inhibitors of glycolysis, 2-DG and 3-bromo pyruvate (BrPA), to adjust glycolytic flux followed by measurement of ^{13}C-lactate, ^{13}C-acetate and ^{13}C-alanine levels following ^{13}C-glucose labeling (Figure 3A). Using these metabolites as readouts, inhibitor levels were titrated so that glycolytic flux was reduced to a level comparable with Meso and DE while avoiding cytotoxicity. Under these conditions, inhibitors promoted loss of pluripotency as indicated by a decrease in the percentage of OCT4$^+$ and SOX2$^+$ cells and *NANOG*, *OCT4*, *SOX2* transcripts within 3 days of treatment (Figure 3B–D and Figure S3A). While DE and Meso marks increased under these conditions, ectoderm markers remained low (Figure S3B). This result is consistent with previous reports showing that elevated glycolytic flux is required for maintenance of hPSCs (Gu et al., 2016; Moussaieff et al., 2015b) but, also suggests that ectoderm differentiation also requires elevated glycolysis.

To address this issue further, directed differentiation to the three germ layers was performed under conditions where aerobic glycolysis was inhibited with 2-DG and BrPA. As anticipated from the previous experiment, treatment with these inhibitors had no impact on DE (Figure 3E–G and Figure S3A) or Meso differentiation (Figure S3C–E). Under ectoderm differentiation conditions however, glycolytic inhibition significantly reduced the up-regulation of *PAX6*, *SOX1* and *SOX2* in NPCs (Figure 3H–J) and *PAX3*, *SOX1* and *SOX2* NCSC (Figure 3K). In the presence of 2-DG and BrPA the percentage of SOX1$^+$ cells was reduced to 8.8% and 22.0%, respectively, while the percentage of PAX6$^+$ cells was <1% under both conditions (Figure 3H,I). We used three approaches to rule out off-target effects for these inhibitors. First, the ectoderm differentiation defect (+2-DG/+BrPA) was rescued by restoring glycolytic flux with galactose and fructose-containing media (Figure S3F–H). Both of these carbon sources enter the glycolysis downstream of the HK step, thereby bypassing the impact of inhibitors in this pathway. Growth on galactose and fructose under these conditions had only a minor impact on growth rates (Figure S3F) and cell cycle profiles (Figure S4A) and NPC lineage markers were maintained indicating that galactose and fructose rescued the effects of inhibitor alone (Figures S3H,I). Second, the pyruvate dehydrogenase inhibitor dichloroacetic acid (DCA) was used to activate OxPhos and suppress aerobic glycolysis in hESCs and NPCs (Figure S4B). Consequently, DCA treatment induced a loss of pluripotency (Figures S4C–E), resulting in the generation of Meso and DE but not ectoderm lineages (Figures S4F–N). Finally 2-DG, BrPA and DCA inhibited the formation of ectoderm but not endoderm and mesoderm in embryoid bodies differentiated from hESCs (Figure S5). Maintenance of elevated glycolytic flux is therefore required for the initial stages of ectoderm differentiation.

Lineage-specific control of metabolic 'switch' genes by MYC/MYCN

Next we set out to understand the mechanism underpinning elevated glycolysis in hPSCs and regulatory steps that control metabolic switching during lineage specification. From the flux analysis, we noted high activities of two key glycolytic enzymes, HK and pyruvate kinase (PK) (Figure 2D); and the enzyme catalyzing the conversion of pyruvate to lactate,

lactate dehydrogenase (LDH) (Figure 2D). All three enzymes have been implicated in metabolic switching in cancer cells (Christofk et al., 2008; Fantin et al., 2006; Patra et al., 2013). In cell lysate-based assays the activities of these enzymes were significantly elevated in hPSCs and NPCs compared to DE, Meso and Fibs (Figure 4A). HK, PK and LDH are therefore likely to be part of the metabolic switch mechanism. Immunoblot analysis of HK isozymes showed that HK1 levels parallel global HK activity in contrast to HK2 which is down-regulated in the three germ layers (Figure 4B). PKLR levels match pyruvate kinase activity in hPSCs and ectoderm but PKM1 levels increase in all differentiated cell types, indicating that it is regulated by post-translational levels of control and may not be a component of the metabolic switch. Finally, both LDH-A/C levels are elevated in hPSCs and ectoderm but not DE, Meso or Fibs. This indicates that both LDH isozymes are potentially part of the metabolic switch mechanism. Changes in the activity of glycolytic enzymes therefore appear to be linked to metabolic changes during cell fate specification. Modulating levels of these enzymes is a potential point of regulation for this.

To investigate if transcriptional regulation was important for control of metabolic activity in hPSCs and during germ layer commitment, 103 transcripts corresponding to genes that encode enzymes involved in glycolysis, the pentose phosphate pathway (PPP), lactate production and other catabolic pathways derived from glycolysis were analyzed from an RNA-seq data set (Table S1). Transcript levels for 85 metabolic genes showed <2-fold change in any germ layer derivative as cells exit pluripotency but, a cohort of 18 transcripts exhibited expression levels that were elevated in hESCs and ectoderm but low in DE and Meso (Figure 4C). The expression pattern of these 18 genes matched the changes in aerobic glycolysis usage within the cell types, i.e. high glycolysis in hPSCs and ectoderm and low glycolysis in DE and Meso, pointing to their potential involvement in metabolic switching. These transcripts encode key glycolytic enzymes (*HK1*, *HK3*, *GAPDHS*, *PGAM2*, *PKLR*, *PKM*), glucose transport (*SLC2A1*), enzymes involved in the PPP (*TALDO1*, *TKT*), lactate production (*LDHA*, *LDHC*, *LDHD*), glycogen biosynthesis (*GPI*, *UGP2*) and glutathione biosynthesis (*PSAT1*) (Figure 4C). Several of these transcripts were validated by qRT-PCR and confirmed to be regulated in a pattern consistent with them being part of the metabolic switch mechanism (Figure 4D). Protein levels for seven of these potential switch enzymes were shown to be regulated in the same manner (Figure 4B). This cohort of genes could potentially be involved in metabolic switching through a transcriptional program.

To understand more about the link between transcriptional regulation and metabolism, we interrogated RNA-seq data to identify transcription factors expressed in hPSCs and ectoderm but not DE or Meso. Two candidates were identified by this strategy; SOX2 and MYCN. By interrogating published ChIP-seq data (Tsankov et al., 2015), 14/18 transcriptionally-regulated genes potentially involved in metabolic switching were bound by MYC in hESCs, whereas only 2 were bound by SOX2. Moreover, 12 of the 14 MYC binding sites were validated via qChIP (Figures 4E–F). The ChIP-seq dataset (Tsankov et al., 2015) only evaluated MYC binding but we used qChIP to confirm that MYCN also occupies the same E-box motif as MYC (Blackwood and Eisenman, 1991) in hESCs (Figure 4E). Although MYCN was lost in DE and Meso, its expression was maintained during early ectoderm differentiation (Figure 4B). Since MYCN and MYC are functionally redundant in a developmental context (Malynn et al., 2000), it is possible that MYC and MYCN regulate

the transcriptional network underpinning the metabolic profile of hPSCs and that MYCN maintains this during early ectoderm differentiation. To establish that ectoderm eventually undergoes metabolic switching we followed the differentiation as NPCs transition to floor plate precursors. During this transition, transcripts for metabolic switch genes coincidently decrease with MYCN transcripts (Figure S2B,C). Metabolic switching occurs during this developmental transition as determined by ^{13}C-NMR analysis (Figure S2D), consistent with MYCN being a major metabolic determinant during development.

MYC activity links metabolic flux to cell fate decisions

The previous data indicate that MYC-family transcription factors control key metabolic genes in hPSCs and that ectoderm specific expression is maintained by sustained MYCN activity. To determine if MYC activity is the critical determinant of metabolic switching, ECARs and OCRs were assayed in MYC-ER hESCs differentiated to DE for 4 days in the absence of 4-hydroxy-tamoxifen (4OHT) or, for the final 2 days in the presence of 4OHT (Figure 5A–C). HK, PK and LDH enzyme activities were also assayed under these conditions (Figure 5D) in addition to pool sizes of intracellular glucose, glycolytic metabolites (glucose-6-P; phosphoenolpyruvate), ribose (PPP), glycogen and lactate by ^{13}C-metabolic labeling analysis (Figure 5E). Induction of MYC during Meso differentiation also results in the restoration of aerobic glycolysis as determined by enzyme activity assays, ^{13}C-flux analysis, and “switch” gene expression (Figure S6B–F). These data show that reestablishment of MYC activity in cells committed to become DE and Meso reverses the metabolic switch that occurs following pluripotency exit. For example, activated MYC-ER restores elevated lactate production, decreases oxygen consumption and restores the activity of key metabolic enzymes to that observed for hESCs (Figure 5B–D). Transcripts for key metabolic genes and protein levels for key metabolic enzymes are reactivated by MYC-ER (+4OHT) (Figures 5F,G), consistent with MYC being the key regulator of metabolic switching. Therefore, metabolic switching occurs under conditions when global MYC activity is low, but is reversed when MYC activity is restored ectopically. However, differentiation to DE or Meso under these conditions was not impacted by MYC re-expression or by reversal of the metabolic switch (Figure S6A–F) and there was no indication that reprogramming occurred under these conditions as indicated by the absence of pluripotency markers (Figure 5F and S6F). This data shows that Meso and DE germ layer formation occurs independently of glycolytic status in contrast to the requirement for elevated aerobic glycolysis in pluripotent cells and during the transition from pluripotency to early ectoderm.

Results described in this report indicate that MYC is a major driver of metabolic flux in pluripotent cells and during early ectoderm differentiation. Because elevated glycolytic flux is required for maintenance of pluripotency and ectoderm commitment (Figure 3), it would be expected that decreased global MYC activity would impact pluripotency and ectoderm differentiation. To address this issue, hESCs and NPCs were transduced with lentivirus to deliver shRNA targeting *MYC* and *MYCN*. Knockdown of *MYC* and *MYCN*, using two distinct shRNAs for each target, significantly decreased levels of pluripotency markers such as OCT4, NANOG and SOX2 (Figure S7A,B). Interestingly, transcripts linked to early Meso (*T*, *GSC*, *GATA4*, *ISL1* and *NKX2.5*) and DE (*T*, *GATA6*, *SOX17*) germ layer formation

were up-regulated following MYC knock-down whereas ectoderm markers (*SOX1, SOX2 and PAX6*) were not (Figure S7C). As expected, metabolic genes targeted by MYC/MYCN (see Figure 4) were significantly down-regulated in hESCs when global MYC activity was decreased (Figure S7C). Coinciding with loss of pluripotency markers, ^{13}C- metabolic flux decreased following knockdown of MYC/MYCN, as shown by reduced lactate, acetate and alanine production (Figure S7D). Knockdown of *LDHA* and *LDHC* in hESCs reproduces the effect of *MYC/MYCN* knockdown, including the loss of pluripotency markers (Figures S7E–F), up-regulation of DE and Meso markers (Figure S7F) and loss of aerobic glycolysis (Figure S7G). This observation is consistent with LDHA's ability to replace MYC as a reprograming factor (Cao et al., 2015), implying that a major role for MYC in reprograming is through metabolic regulation. These findings support the hypothesis that MYC-regulated metabolic activity is required for maintenance of pluripotency.

Similar experiments were then performed to investigate whether elevated MYCN activity was required for early ectoderm differentiation. These experiments show that maintenance of elevated MYCN activity is required for up-regulation of NPC-specific markers PAX6 and SOX1 and maintenance of *SOX2* expression under ectoderm differentiation conditions (Figure 6A,B). This is accompanied by increased expression of Meso and DE transcripts (Figure 6C). Transcripts for metabolic 'switch' genes are significantly decreased when MYCN activity is reduced (Figure 6C) and ^{13}C-metabolic flux is also significantly reduced compared to controls (Figure 6D). This indicates that when MYC activity is low, elevated glycolytic activity is not maintained and cells switch lineage choice away from an ectoderm fate. As seen in hESCs, knockdown of *LDHA/LDHC* blocks NPC differentiation and induces a metabolic shift (Figures 6E–G), reproducing the effects seen following *MYCN* knockdown and glycolytic inhibition. Overall this supports our model (Figure 7) where MYC/MYCN activity maintains pluripotency and the transition to ectoderm by maintaining glycolytic flux through transcriptional regulation of metabolic 'switch' genes. Importantly, this defines MYC/MYCN as a regulator of lineage choice by linking cell fate decisions to metabolic flux.

DISCUSSION

Metabolic switching is thought to occur as cells exit the pluripotent state (Gu et al., 2016; Moussaieff et al., 2015b; Varum et al., 2011; Zhang et al., 2011). Our study however, reveals that metabolic switching is not a requirement for PSCs to initiate differentiation and reveals that metabolic control during germ layer formation is far more dynamic than previously recognized. The assumption that PSCs switch from a glycolytic mode of energy generation to one more dependent on OxPhos is based on previous studies comparing fully differentiated cells, embryoid bodies or non-ectoderm lineages such as DE. Overlooking metabolic regulation in the early ectoderm lineage has therefore led to the erroneous assumption that metabolic switching is an integral part of pluripotency exit. Besides the requirement for high glycolytic flux in pluripotent cells, we show that transition to the early ectoderm germ layer also requires elevated glucose oxidation. This is not the case in DE and Meso that heavily utilize OxPhos for their energy requirements. Cells fated to become neural cells switch their metabolic activity at the midbrain floor plate stage of differentiation, just after they have transitioned through a neural progenitor cell state (Zheng et al., 2016).

Interestingly, neural progenitors from the sub-ventricular zone, but not mature neurons, have a high glycolytic rate but undergo switching during neuronal maturation (Candelario et al., 2013). Mechanisms driving metabolism-linked ectoderm development *in vivo* may therefore be related to the ones identified by us in this report. It should be noted that the MYC/MIZ-1 regulatory axis performs an important role in adult neural stem cells function *in vivo* (Adhikary et al., 2003; Kerosuo et al., 2008) although this seems to be through regulation of cell proliferation.

A major question arising from our work is why elevated aerobic glycolysis is required for maintenance of pluripotency and ectoderm specification. SOX2 is of potential interest because it is expressed in pluripotent cells and in early ectoderm lineages, both of which have elevated aerobic glycolysis. Of note, SOX2 is subject to O-GlcNacylation, a post-translational modification directly impacted by metabolic flux through the hexosamine biosynthetic pathway (Myers et al., 2016). Alternatively, glutathione-dependent redox state could impact the activity of ectoderm-specific transcription factors. Both of these scenarios and others could be impacted by the metabolic regulation described in this report.

Our work indicates that metabolic activity is mechanistically linked to the pluripotent state and cell fate decisions made by PSCs. This concept is likely to apply to a broader range of biological scenarios based on several reports linking dynamic metabolic regulation to normal developmental processes. During cardiomyocyte maturation for example, energy generation switches from a glycolytic to Ox-Phos-dependent mechanism (Lopaschuk and Jaswal, 2010). A similar observation has been made as NPCs transition to neurons in culture (Zheng et al., 2016). During mammalian development the WNT, Sonic hedgehog and Notch signaling pathways link cell fate decisions to metabolic switching in cell types such as brown fat, skeletal muscle and bone (Esen et al., 2013; Teperino et al., 2012). Skeletal muscle stem cells undergo a metabolic switch to an OxPhos metabolism as they enter quiescence postnatal; however, injury cues can induce metabolic remodeling back to aerobic glycolysis that drives re-entry into the cell cycle and regenerative capabilities (Ryall et al., 2015b). In breast cancer cells, Notch signaling induces glycolysis and promotes aggressive tumor growth, linking metabolism to disease pathogenesis (Landor et al., 2011). Deregulated metabolic switching has also been implicated in obesity and type-II diabetes (Vander Heiden et al., 2009), raising the possibility that metabolic switching is important not only for developmental decisions but also for disease pathogenesis. Numerous reports have also described the requirement for a glycolytic mode of metabolism to reprogram fibroblasts to a pluripotent state (Cliff and Dalton, 2017; Folmes et al., 2011; Kida et al., 2015; Ryall et al., 2015a). This metabolic need underscores observations described in this report and elsewhere (Gu et al., 2016; Moussaieff et al., 2015b) that glycolytic flux is linked, but not limited, to maintenance and establishment of the pluripotent state. Understanding metabolic switching at the molecular level is therefore critical for a better understanding of development and disease progression.

The assumption that metabolic switching is an inherent feature of pluripotency exit and germ layer entry has led to numerous models attempting to link metabolism with cell fate decisions. One idea that has received significant attention has been the impact of metabolic changes on epigenetic modifications that can potentially regulate global or specific patterns

of gene regulation to elicit cell fate changes (Moussaieff et al., 2015a; Shyh-Chang and Daley, 2015). Here, high glycolytic flux elevates levels of acetyl CoA that contributes to increased histone acetylation and, as a consequence, maintenance of pluripotency. Other reports link metabolism to pluripotency maintenance mechanisms by showing that elevated levels of methionine biosynthesis contribute to epigenetic modifications through generation of S-adenosylmethionine (SAM) (Shiraki et al., 2014). Both mechanisms have been proposed to contribute to pluripotency maintenance and the regulation of differentiation. Although generating elevated levels of acetate/acetyl CoA and SAM may be important for pluripotency, metabolic switching and reduced synthesis of these metabolites does not appear to be required for pluripotency exit for all germ layers. Two reports have shown that histone acetylation and methylation marks are resolved as PSCs transition to nascent ectoderm (Golebiewska et al., 2009; Qiao et al., 2015). The connection between elevated aerobic glycolysis and epigenetic regulation in ectoderm is therefore unclear because our data indicates that epigenetic changes proceed under conditions where aerobic glycolysis remains elevated. It is possible that metabolism-driven epigenetic modifications are important for cell fate transitions but analysis of global histone levels, for example, can be misleading and more targeted analysis is required to understand this connection.

In this report, we show that expression of MYC family members is a major determinant of pluripotency and cell fate. Although MYC is recognized to be critical for maintenance of PSCs (Cartwright et al., 2005; Smith et al., 2010; Varlakhanova et al., 2010) specific roles for MYC in pluripotency have been difficult to identify although roles in cell cycle regulation and metabolism have been proposed (Kim et al., 2010; Lin et al., 2009; Smith et al., 2010). Here, we show that MYC performs a critical role in pluripotency by maintaining the activity of a cohort of metabolic genes that we refer to as 'switch' genes. Reduced MYC and MYCN activity in DE and Meso lineages provides a basis for explaining how metabolic switching occurs in these germ layers. Moreover, maintenance of 'switch' genes by MYCN during ectoderm differentiation provides a mechanism for how a pluripotent mode of metabolism is retained in this lineage. The requirement to maintain elevated glycolysis for ectoderm specification therefore establishes MYCN as a developmental regulator through its ability to control metabolism. Although MYC is a well-established transcriptional regulator of metabolic genes (Hsieh et al., 2015; Stine et al., 2015), its role in metabolic switching during development has not been previously recognized. This is the first report to identify a role for MYC as a regulator that links metabolism to cell fate decisions. These observations have broad implications because MYCs role in coupling metabolism to cell fate has obvious implications for disease pathogenesis including cancer, diabetes and obesity.

CONTACT FOR REAGENT AND RESOURCE SHARING

Further information and requests for resources and reagents should be directed to and will be fulfilled by the Lead Contact, Stephen Dalton (sdalton@uga.edu).

EXPERIMENTAL MODEL AND SUBJECT DETAILS

Cell culture and differentiations

Human embryonic stem cell (hESCs) lines WA07 (Sex: male, WiCell, WAe007-A), WA09 (Sex: female, WiCell, WAe009-A), Cyt49 (Sex: male, ViaCyte Inc.) and induced pluripotent stem cell (hiPSC) line K3 (Sex: male), a gift from Stephen Duncan (Si-Tayeb et al., 2010) were cultured as described previously (Singh et al., 2015). hESCs and hiPSCs were seeded at 50,000 cells/cm^2 on polystyrene culture plates coated with Geltrex LDEV-Free hESC qualified reduced growth factor basement membrane matrix (ThermoFisher, A1413302) at a 1:200 dilution in DMEM/F-12 w/o glutamine (Corning, 15–090-CM). A chemically defined base media (DM) was comprised of DMEM/F-12 w/o glutamine supplemented with 2% Probumin (EMD Milipore, 821005), 1× Antibiotic-Antimyotic (Corning, 30-004-CI), 1× MEM non-essential amino acids (Corning, 25-025-CI), 1× Trace Elements A (Corning, 99–182-CI), 1× Trace Elements B (Corning, 99–175-CI), 1× Trace Elements C (Corning, 99–176-CI) 50 ug/mL ascorbic acid (Sigma, A8960), 10 ug/mL Transferrin (Athens Research and Technology, 16-16-A32001-LEL), 0.1 mM 2-mercaptoethanol (Gibco, 21985023) and 1× Glutagro (Corning, 25-015-CI). DM was then supplemented with 8 ng/mL human basic-FGF (R&D Systems, 4114-TC), 200 ng/mL LONG® R3 human IGF-I (Sigma, 85580C), 10 ng/mL Activin A (R&D Systems, 338-AC-01M/CF) and 10 ng/mL human Heregulinβ-1 (Peprotech, AF-100-03) to comprise a complete defied media (CDM). hESCs and hiPSCs were cultured in CDM with media changes every 24 hr to 90% confluency, ~4 days, with 5% CO_2 in a 37 °C incubator. hESCs and iPSCs were removed from culture plates for passaging using Accutase (Innovative Cell Technologies, AT 104) at room temperature (RT) for 5–10 min. Following centrifugation at 1000 rpm for 4 min at RT, Accutase was aspirated off and the cell pellet was resuspened in CDM, then cell number was quantified with a hemocytometer. Cells were reseeded onto Geltrex-coated plates as described above. Positive expression of OCT3/4, SOX2 and NANOG via real time-quantitative polymerase chain reaction (qRT-PCR), immunofluorescence or flow cytometry confirmed cell identity.

Definitive endoderm (DE) cells were generated by culturing hESCs or hiPSCs at 50,000 cells/cm^2 on Geltrex, diluted 1:200 with DMEM/F-12, coated plates for 4 days in DM supplemented with 100 ng/mL Activin A and 8 ng/mL human basic-FGF, with 25 ng/mL human Wnt-3a (R&D Systems, 1324-WN-500/CF) added to the media for the first 24 hr only. Media was changed every 24 hr. Positive expression of SOX17, FOXA2, GATA6 and GSC via qRT-PCR, immunofluorescence or flow cytometry with negative expression of OCT3/4, SOX2 and NANOG confirmed cell identity. Cell culture methods were as described previously (Singh et al., 2015).

Nascent mesoderm (Meso) cells were generated by culturing hESCs or hiPSCs at 50,000 cells/cm^2 on Geltrex, diluted 1:200 with DMEM/F-12, coated plates for 4 days in CDM supplemented with 25 ng/mL human Wnt-3a and 100ng/mL human BMP-4 (R&D Systems, 314-BP-05M/CF). Media was changed every 24 hr. Positive expression of ISL1, GATA4 and NKX2.5 via qRT-PCR, immunofluorescence or flow cytometry with negative expression of OCT3/4, SOX2 and NANOG confirmed cell identity. Cell culture methods were as described previously (Berger et al., 2016).

Neural progenitor cells (NPC) were generated by culturing hESCs or hiPSCs at 90,000 cells/cm^2 on Geltrex, diluted 1:200 with DMEM/F-12, coated plates for 6 days in DM supplemented with 10 ng/mL human Heregulinβ-1, 200 ng/mL LONG® R3 human IGF-I, 20 μM SB431542 (R&D Systems, 1614/10) and 500 nM LDN (Sigma, SML0559). Media was changed every 24 hr. Positive expression of PAX6, NES, TUBB3, SOX1 and SOX2 via qRT-PCR, immunofluorescence or flow cytometry with negative expression of OCT3/4, SOX2 and NANOG confirmed cell identity. Cell culture method was adapted from a previously published protocol (Chambers et al., 2009).

Pre-neural crest stem cells (NCSC) were generated by culturing hESCs or hiPSCs at 90,000 cells/cm^2 on Geltrex, diluted 1:200 with DMEM/F-12, coated plates for 6 days in DM supplemented with 10 ng/mL human Heregulinβ-1, 200 ng/mL LONG® R3 human IGF-I, 8 ng/mL human basic-FGF, 20 μM SB431542 and 0.2 μM BIO (R&D Systems, 3194/10). Media was changed every 24 hr. Positive expression of PAX3, SOX1 and SOX2 via qRT-PCR, immunofluorescence or flow cytometry with negative expression of OCT3/4, SOX2 and NANOG confirmed cell identity. Cell culture method was described previously (Menendez et al., 2013).

Human foreskin fibroblasts (Fibs) CCD-1079Sk (Sex: male, ATCC®, CRL-2097) and HEK293FTs (Sex: female; Life Technologies, 31985) were grown on plastic culture plates in a growth media consisting of DMEM (Corning, 10–013-CM) with 1× Antibiotic-Antimyotic, 1 mM sodium pyruvate (Corning, 25-000-CI) and 20% fetal bovine serum (Atlanta Biological, S10250), with media changes every 48 hr. Fibs were grown to confluency and then split with trypsin-EDTA (Sigma, T4049) and re-seeded at a 1:8 dilution. These Fibs were the source of cells from which K3 hiPSC were made.

Cell counts for doubling times were determined following 2, 3 and 4 days of culture for hESCs, DE and Meso and after 4, 5 and 6 days for NPCs and NCSCs. Cells were dissociated with Accutase and quantitated via hemocytometer in two independent counts. Doubling times were calculated with the following formula: doubling time = (time*log(2))/(log(final cell number)-log(initial cell number)).

To generate embryoid bodies, 5.5 million WA09 hESCs were aggregated into spheres in a 6-well plate on an Innova2000 orbital rotator (New Brunswick Scientific) at 97 rpm for 16 hr in their normal culture media with 10 μmol Y-27632 dihydrochloride (R&D Systems, 1254/50), a Rho-kinase inhibitor to aid aggregation. Following aggregation, media was changed to DMEM with 1× Antibiotic-Antimyotic, 1 mM sodium pyruvate and 20% fetal bovine serum (Sigma, F6178), media was changed every 48 hr. Bright field images were taken every 2 days along with an aliquot of spheres for qRT-PCR analysis.

Hexokinase inhibitors 2-deoxyglucose (2-DG)(Santa Cruz, sc-202010A) and 3-bromopyruvate (BrPA)(Santa Cruz, sc-260854A) were used at 2.2 mM and 17μM, respectively, for long-term cell culture 1–16 days. Pyruvate dehydrogenase kinase inhibitor dichloroacetic acid (DCA)(Sigma, D54702) was used at 2.5 mM for long-term cell culture 1–16 days, with sodium hydroxide used to balance pH.

METHOD DETAILS

MYC-ER Experiments

The human MYC open reading frame was cloned in-frame with truncated estrogen receptor under the control of the pCAG promoter as described previously (Cartwright et al., 2005). WA09 cells were seeded and grown for 2 days as described above in a 6-well plate, and 2.5 μg of the MYC-ER plasmid was transfected in the WA09s with Lipofectamine 3000 (Invitrogen, L3000015) using the manufacture's protocols. Transfected cells were selected with puromycin at 200 μg/mL in CDM 24 hr after transfection. After 3 days of puromycin selection large amounts of cell death necessitated the passaging of transfected cells to 4 wells of a 24-well plate, and after an additional 2 days of selection the cells were passaged again to a single 24 well. Following this passage cell death subsided and the transfected cells began to amplify and 3 days later were able to be expanded under drug selection and then clonally expanded. MYC-ER expressing WA09 cells (MYC-ER) were seeded and maintained under normal WA09 growth conditions and differentiated to DE and Meso linages as described above. 4OHT at 1 μM (Sigma, H7904) in DMSO was used to induce MYC-ER activation during final 48 hours of cell culture.

Seahorse Metabolic Analysis

hESCs, hiPSCs, Fibs, DE, Meso and MYC-ER cells were plated on Seahorse XFe24 cell culture microplates (Agilent, 100777-004) under conditions described above for 4 days. NPCs and NCSCs were plated on XFe24 cell culture microplates and grown for 6 days for NPCs as described above. Growth media for each cell type was changed to Seahorse XF Base Medium (Agilent, 102353-100) supplemented with 1 mM Glutagro, and cells were placed in a non-CO_2 incubator 1 hr prior to assay. Extracellular acidification rates (ECAR) and oxygen consumption rates (OCR) were measured via the glycolytic stress test assay (Agilent, 103020-100) with a Seahorse XFe24 Analyzer (Agilent) following the manufacturer's protocols. Following Seahorse analysis cells were lysed with RIPA buffer (Sigma, R0278) and protein content measured by Bradford assay. Data was processed via Wave software (Agilent) and standardized to protein content. The glycolytic rate measurements were calculated as the difference in ECAR measurements before and following glucose injection and glycolytic capacity measurements were calculated as the ECAR measurements flowing oligomycin treatment subtracted by the initial background measurements, as described by provided protocol (Agilent, 103020-100). OCR rates were calculated as the difference in OCR measurements following glucose injection and the OCR measurements following oligomycin injection.

Immunostaining

Cells were washed with DPBS (Corning, 21–031-CM) and fixed with a 4% paraformaldehyde (Electron Microscopy Sciences, 15710) in DPBS solution for 15 min. After 3 washes with DPBS cells were blocked with a 10% donkey serum (Equitech-Bio, SD30–0500), 0.2 M Triton X-100 (Fisher Scientific, BP151–500) and 0.3 M glycine (Sigma, G8898) in DPBS solution for 1 hr at RT. Primary antibodies, see Table S2, were prepared in a 10% donkey serum, 0.2 M Triton X-100 in DPBS solution and incubated overnight at 4 °C. After 3 washes with DP BS, secondary antibodies, see Table S2, in a 2.5% donkey

serum, 0.2 M Triton X-100 in DPBS solution were incubated for 1 hr at room temperature in the dark. Following removal of secondary antibody, 1 μg/mL 4,6-Diamidino-2-phenylindole dihydrochloride (Sigma, D9542) in DPBS was added to cells for 5 mins. After 3 washes in DPBS, coverslips were mounted to slides with ProLong Diamond Antifade (ThermoFisher, P36961). A Leica DM6000B microscope and Zeiss LSM 710 confocal microscope were used to obtain images. Images were processed with Slidebook 6 (Intelligent Imaging Solutions) and cell counts were analyzed with Image J (Schneider et al., 2012).

qRT-PCR

Cells were harvested with a cell scraper in ice cold DPBS and pelleted by centrifugation at 1000 rpm for 4 min at RT. E.Z.N.Z RNA isolation kit (Omega, R6834-02) was used to isolate RNA following the manufacturer's protocols and the RNA quantitated with a Biotek Synergy 2 plate reader. cDNA was synthesized with 1 μg of RNA using the Iscript cDNA synthesis kit (Bio-Rad, 1708841) following the manufacturer's protocols. The cDNA was then diluted to a final volume of 500 μL with molecular grade water. Δ ΔCt qRT-PCR analysis was performed on a ViiA7 Real-Time PCR System (Life Technologies) in a 384 well plate with a reaction of 5 μL TaqMan Universal PCR Master Mix No AmpErase UNG (ThermoFisher, 4324020), 0.5 μL TaqMan primer (Life Technologies), 0.5 μL molecular grade water and 4 μL cDNA, see Table S3 for primers. Expression of each transcript was normalized to 18S ribosome, performed in triplicate and plotted as the mean ± standard deviation.

qChIP

Washing buffer, consisting of 0.5% (w/v) BSA (Sigma, A4503), was used for 3 washes 1.5 mg of Dynabeads Protein G (Life Technologies, 10004D). Antibodies, see Table S2, were conjugated to beads in 200 μL of washing buffer and rotated for a minimum of 4 hrs at 4 °C. Cells were dissociated with Accutase a nd quantitated with a hemocytometer. Approximately 20 million cells were washed with DPBS and crosslinked in 1% methanol-free formaldehyde (ThermoFisher, 28906) in DPBS for 10 min while rotating at RT. Crosslinking was quenched in 200 mM glycine in DPBS for 5 min while rotating at RT and washed twice with ice cold DPBS. Cells were pelleted and stored at −80 °C. Crosslinked cell pellets were resuspended in 1 mL of lysis buffer consisting of 10 mM Tris-HCl ph 8.0 (Life Technologies, 15568-025), 100 mM NaCl (Life Technologies, AM9760G), 1 mM EDTA (Life Technologies, AM9260G), 0.5 mM EGTA (Sigma, E3889), 0.1% Na-Deoxycholate (Sigma, 30970), 0.5% N-lauroylsarcosine (Research Organics, 9603L) and 1× protease inhibitors (Sigma, 11836170001), for 30 min on ice. Lysates were sonicated in a 1 mL milliTUBE (Covaris, 520081) on a Covaris S220 for 20 min at 200 cycles/burst, a peak power of 140 and a duty factor of 5%. Sonicated lysates were supplemented with 1% Triton X-100 and centrifuged at max speed for 5 min at 4 °C. The resulting supernatant was split into 300 μL aliquots with 10 μL of the supernatant collected as input. Antibody conjugated beads were washed 3 times with washing buffer and then added to a 300 μL aliquot of sonicated lysate and incubated overnight at 4 °C while rotating. Beads were washed twice with 1 mL of 20 mM Tris-HCl ph 7.4 (Life Technologies, 15567-027), 150 mM NaCl, 0.1% SDS (KD Medical, CUS-0301), 1 % Triton X-100 and 2 mM EDTA and then washed twice with 1 mL of 10 mM Tris-HCl ph 7.4, 250 mM LiCl (Sigma, L4408), 1% Triton X-100,

0.7% Na-Deoxycholate and 1 mM EDTA. Finally, beads were washed twice with 1 mL of 10 mM Tris-HCl ph 8.0, 0.2 % Tween-20 (Sigma, P7949) and 1 mM EDTA. Crosslinking was reversed by incubating beads in 100 μL of 10 mM Tris-HCl pH 8.0, 0.5% SDS, 300 mM NaCl, 5 mM EDTA and 3.2 units of Proteinase K (Roche, 3115828001) for 1 hr at 55 °C followed by 8 hr at 65 °C. ChIP-DNA was recovered from the uncrosslinke d supernatant with a MinElute PCR kit (Qiagen, 28004) following the manufacturer's protocol and diluted to a final volume of 150 μL with molecular grade water. ChIP-DNA was quantified by qRT-PCR on a ViiA7 real time PCR system in a reaction consisting of 4 μL DNA, 5 μL SYBR Green (Kapa Biosystems, KK 4602), 0.5 μL of 10 mM right primer, 0.5 μL of 10 mM left primer and 0.2 μL of Rox Low (Kapa Biosystems, KK 4602). See Table S4 for primers.

Enzyme Activity Assays

Cells from a 10cm plate were dissociated with Accutase and aliquoted into 4 samples, three for enzyme activity analysis and the other for protein content determination. Cells were pelleted in each aliquot by centrifugation at 1000 rpm for 4 min at RT. The hexokinase colorimetric assay (Sigma, MAK091-1KT) and pyruvate kinase activity assay (Sigma, MAK091-1KT) were performed as recommended by the manufacturer. Cell lysates for lactate dehydrogenase (LDH) activity assays were prepared by re-suspending cell pellets in 100 mM sodium phosphate pH 7.5 at 37 °C with 1.0% (w/v) bovine serum albumin (Sigma, A4503) followed by lysing with three freeze-thaw cycles (Sekine et al., 1994). LDH activity in cell extracts was determined by measuring the loss NADH at A_{340nm} as previously described (Bergmeyer et al., 1974). Assay buffer sformulation consisted of 100 mM sodium phosphate pH 7.5 at 37 °C, 1.0% (w/v) bovine serum albumin, 121 μM NADH (Sigma, N8129) and 1.13 mM sodium pyruvate (Sigma, P2256). Enzyme activities were standardized to protein content and reported in units of mU/μg of protein, where one unit is the amount of enzyme activity that will reduce 1 μmol of pyruvate to lactate at pH 7.5 and 37 °C.

Intracellular Flow Cytometry

Cells were dissociated using Accutase for 10 minutes, washed with sterile DPBS and pelleted at 200 × g for 4 minutes. Cells were resuspended in 0.5 mL of Flow Cytometry Fixation Buffer (R&D Systems, FC009) and incubated at room temperature for 10 min. Following fixation in 1% formaldehyde cells were washed twice with DPBS, pelleted and resuspended in 200 μL of Flow Cytometry Permeabilization/Wash Buffer I (R&D Systems, FC009). Primary antibodies, see Table S2, were incubated with fixed cells for one hour at 4 °C. Cells were then washed and incuba ted with secondary antibodies, see Table S2, for 30 minutes at 4 °C. Analysis was perf ormed on a Beckman Coulter CyAn and the results were analyzed and plotted using FlowJo v10.

Cell Cycle Profiling

Cells were pulse-labeled with 10 μM 5-ethynyl-2'-deoxyuridine (EdU) for 30 minutes for hESCs or, 1 hr for differentiated cells, to label actively replicating DNA. The cells were then fixed and EdU labeling was detected using the Click-iT Plus Edu Flow Cytometry Assay kit (Invitrogen, C10634) at room temperature protected from light. Then, cells were stained with FxCycle Violet at 1 μL/mL (Life Technologies, F10347) to measure DNA content for

30 minutes at room temperature protected from light. EdD labeling and DNA content were analyzed using a Beckman Coulter CyAn ADP flow cytometer.

Western Blotting

Cells were washed with ice cold DPBS, collected with a cell scrapper, pelleted via centrifugation at 1000 rpm for 4 min, flash-frozen in liquid nitrogen and stored at −80 °C as cell pellets. Cell pellets were resuspened and lysed on ice for 30 min in 50 μL of a buffer consisting of RIPA lysis buffer (Sigma, R0278), 1× protease inhibitor, 1× phosphatase inhibitor (EMD Millipore, 524625) and 100 mM dithiothreitol (Sigma, D9779). Lysates were centrifuged at 20,000 × g for 10 min at 4 °C with the supernatant collected. Protein concentrations of supernatants were determined by Bradford assay at 595 nm on a Biotek Synergy 2 and diluted 1:1 with Laemmli buffer (Bio-Rad, 161–0737) supplemented with 5% 2-mercaptoethanol. Bolt Bis-Tris precast gels (Life Technologies, NW00080BOX) were loaded with 30 μg of protein and separated by electrophoresis at 165 V for 35 min. Protein was transferred to a nitrocellulose membrane via a Bolt transfer system (Life Technologies) at 10 V for 60 min. Membranes were blocked with a solution of 2% nonfat blocking milk (Bio-Rad, 170–6404) in TBST, 0.5% (v/v) Tween-20 in 25 mM TBS, for 1 hr at RT while rocking followed by 3 washes with TBST. Primary antibodies, see Table S2, were added to membranes in blocking solution and incubated overnight at 4 °C while rocking. Following incubati on, membranes were washed 3 times in TBST for 5 min at RT while rocking. Secondary antibodies, see Table S2, were added to membranes in blocking solution and incubated for 1 hr at RT while rocking and then washed with TBST three times. Protein levels on membranes were detected with Amersham ECL detection kit (GE, RPN2106) with Amersham hyperfilm (GE, 28–9068-35).

shRNA Knockdowns

shRNAs targeting *MYC* (Sigma, SHCLNG-NM_002467 TRCN0000353004 and SHCLNG-NM_002467 TRCN0000039642), *MYCN* (Sigma, SHCLNG-NM_005378 TRCN0000020694 and SHCLNG-NM_005378 TRCN0000358465), *LDHA* (Sigma, SHCLNG-NM_005566 TRCN0000164922 and SHCLNG-NM_005566 TRCN0000159591) and *LDHC* (Sigma, SHCLNG-NM_017448 TRCN0000160531 and SHCLNG-NM_017448 TRCN0000026556) were packaged into virus using HEK293FT cells (R700-07, Life Technologies). HEP293FT cells were seeded at 122,000 cells/cm^2 in Opti-MEM Reduced Serum Media (Life Technologies) and transfected with Lipofectamine 3000, ~1.5 μg/mL shRNA plasmids, 675 ng/mL pMD2.G (a gift from Didier Trono, Addgene plasmid # 12259), 450 ng/mL psPAX2 (a gift from Didier Trono, Addgene plasmid # 12260) and 3.6 μL/mL P3000 Enhancer Reagent (Invitrogen, L3000-015). Media was collected 24 and 48 hr after transfection and pooled. Virus within collected media was concentrated with Lenti-X Concentrator (Clontech, 631231) using provided protocols. WA09 cells were plated at 72,000 cells/cm^2, or 129,000 cells/cm^2 for NPC differentiation, and transduced 24 hrs after plating with virus with an MOI of 2 in 6 μg/μL polybrene. One day after transduction cells were selected with 3 μg/mL puromycin for 2 or 4 days for hESCs and NPCs, respectively.

RNA-Seq and Multidimensional Scaling Analysis

For RNA sequencing, total RNA samples were collected and purified using E.Z.N.A Total RNA kit and were DNase treated on-columns using RNase-free DNase set (Omega, E1091). Total RNA quality was confirmed using a 2100 bioanalyzer. Samples with an RIN > 9 were processed for RNA-Seq. An average of 25 million paired-end reads with a length of 50 bp were generated per library on a HiSeq 2500 platform by Hudson Alpha (Huntsville, Alabama). Reads were mapped to the human genome (hg19) by TopHat v2.0.13, (Kim et al., 2013), using the following parameters: no-novel-juncs, max-multihits 1, solexa-quals and no-coverage-search -r 200. Differential gene expression analysis was preformed using Cufflinks (Trapnell et al., 2012) utilizing the default set. A gene was considered to be differentially expressed when the fold-change was greater than 2 and the p-value was smaller than −0.05.

Multidimensional scaling (MDS) was performed on published and our RNA-Seq data using R packages limma (Ritchie et al., 2015) and edgeR (McCarthy et al., 2012; Robinson et al., 2010). Gene read counts (FPKM) were summarized by featureCounts. Genes expressed in more than 3 datasets and with a variance in transcript level (log2(FPKM)) greater than 1 were utilized were utilized for MDS analysis. Subsequently, we set the 20^{th} percentile of the read counts as minimal detection threshold. Genes having read counts below this threshold value were removed from MDS plotting. MDS plots were generated using Glimma (Su et al., 2017). Data sets utilizing a comparable differentiation scheme and timeline were available as paired-end experiments for hESCs, DE and Meso; while only single-end experiments were avaialable for NPCs. There were no pre-NCSC RNA-seq data sets publicly available; therefore the NCSCs could not be utilized in this analysis.

Media for Metabolic Flux Labeling

Uniformly labeled ^{13}C-glucose (Cambridge Isotopes, CLM-1396) at 3.151 g/L was added to glucose-free DMEM/F12 (US Biological, D9807-02) to prepare ^{13}C-glucose DMEM/F-12 base media for metabolic flux analysis. For ^{13}C-glucose DMEM base media, 4.5 g/L uniformly labeled ^{13}C-glucose and 3.7 g/L of $NaHCO_3$ (J.T. Baker, 3506-01) was added to glucose-free DMEM (Sigma, D5030). DMEM/F-12 ^{13}C-galactose and DMEM/F-12 ^{13}C-fructose base media were created by adding 3.151 g/L uniformly-labeled ^{13}C-galactose (Cambridge Isotopes, CLM-1570) or 3.151 g/L uniformly-labeled ^{13}C-fructose (Cambridge Isotopes, CLM-1553), respectively, to glucose-free DMEM/F12. Uniformly labeled ^{13}C-galactose or uniformly labeled ^{13}C-fructose at 4.5 g/L was added to glucose-free DMEM to prepare DMEM ^{13}C-galactose and DMEM ^{13}C-fructose base media. The ^{13}C-labeled DMEM/F-12 was substituted for normal DMEM/F-12 in the BM preparations for hESC, hiPSC, DE, Meso, NPC and NCSC media formulations described above to create cell-type specific ^{13}C-labeling media. The ^{13}C-labeled DMEM was substituted for the normal DMEM for Fibs culture medium as described above.

Labeling of Cells for Metabolic Flux Analysis

To ensure at least 20 million cells were utilized for metabolic flux analysis, ^{13}C-labeling was performed on 10 cm culture plates. Following 4 days of hESCs, hiPSCs, DE, Meso or Fibs culture with cell-type specific growth medium, media was exchanged with cell-type

specific ^{13}C-labeling medium and incubated for 0, 1, 2, 3 or 4 hrs. This was done following 6 days of culture for NPCs and NCSCs. Following labeling for 0–4 hrs, spent ^{13}C-labeling medium was collected and cells were washed with cold DPBS. To determine the number of cells within each culture plate, cells were removed from a 0.25 cm^2 section of the plate with a cell scraper, isolated into single cell solutions with Accutase and quantitated with a hemocytometer. Cells were collected from the remaining portion of culture plates with a cell scraper, pelleted via centrifugation at 1000 rpm for 4 min, flash frozen in liquid nitrogen and stored as cell pellets at −80 °C.

Pelleted cells were lysed by cytolysis by adding 250 μL of molecular grade water to frozen cell pellets in 15 mL conical tubes and thawed on ice for 20 min. The cell lysate was separated into aqueous and organic phases via a Bligh-Dyer extraction (Miccheli et al., 2006). In detail, 750 μL of a 2:1 chloroform:methanol mixture was added to each lysate, followed by 250 μL of methanol, and then 250 μL of molecular grade water. Between each addition, samples were mixed by vortexing at maximum intensity. Lysate solutions were then centrifuged at 3000 × g in a Sorvall Legend RT at 4 °C; resolving the lysate into two clear phases se parated by a solid white precipitate. The top phase contained aqueous metabolites that were recovered with a pipette and transferred to a fresh microcentrifuge tube. The organic bottom phase was recovered by inserting a pipette into the bottom of the conical tube and slowing drawing up the liquid and transferred to a fresh microcentrifuge tube. The precipitate was discarded.

The aqueous and organic samples, along with the 1 mL of media samples, for each sample were concentrated by lyophilization, thereby removing ^{1}H protons. A 10 mM stock of 3-(Trimethylsilyl)-1-propanesulfonic acid (DSS) (Sigma, 178837) was prepared with D_2O (Cambridge Isotopes, DLM-6) as the solvent; the DSS was used as a chemical shift standard for NMR spectroscopy. The aqueous and media samples were resuspened with 153 μL of D_2O and 17 μL of the 10 mM DSS stock to bring the final volume to 170 μL. The organic samples were resuspened in 170 μL of $CDCl_3$ (Cambridge Isotopes, DLM-7), with the $CDCl_3$ as the chemical shift standard. The aqueous and media samples were stably stored at −20 °C for at least one year, however the organic samples were analyzed immediately as they were not stable at −20 °C for more than 48 hr. Each sample was loaded into a 3 mm glass NMR tube (Wilmad LabGlass, 335-PP-7) for analysis. Each sample was analyzed on a 63 mm bore 800 MHz spectrometer (Varian/Agilent) with VnmrJ software (Agilent) by collecting a gradient enhanced 1D-^{1}H and 2D-^{1}H, ^{13}C-heteronuclear single quantum coherence (cCHSQC) spectra, from the Varian/Agilent BioPack software. Acquisition time for the aqueous samples was 6 hr with a recycling time of 1.5 hr. The organic samples had an acquisition time of 4.5 hr and 1.25 hr recycling time; and the media samples had a 30 min acquisition time with a 7.5 min recycling time. Each spectra was processed using Mnova software (Mestrelab Research). Each peak within the cCHSQC spectrum was integrated relative to DSS for aqueous and media samples or $CDCl_3$ for organic samples so that spectra could be standardized. Peaks within the cCHSQC spectrum represent individual C-H bonds within metabolite compounds and were identified using chemical shift data from the Human Metabolome Database and Biological Magnetic Resonance Data Bank (Ulrich et al., 2008; Wishart et al., 2013). The integrated values for each identified metabolite within a spectrum were transformed to mass quantities through a standard curve. Standards (Table S5) were

prepared in 170 μL of $CDCl_3$ or D_2O with 1mM DSS to concentrations of 9.03 mM, 45.17 mM, 90.33 mM, 451.67 mM and 903.34 mM. Due to the 1.107% natural abundance of ^{13}C this is equivalent to concentrations of 0.1 mM, 0.5 mM, 1.0 mM, 5.0 mM and 10 mM, respectively, of ^{13}C-labeled metabolites to be used in a standard curve. Peak intensities within standard spectra were integrated relative to DSS or $CDCl_3$, then plotted in a standard curve of concentration vs. intensity and used to transform sample peak intensities into concentration values. The concentration values for each peak were then transformed into mass quantities using the known sample volume of 170 μL. The mass quantity for each peak was then standardized to 25 million cells and plotted on a mass accumulation vs time plot for each peak in each cell type using the other time point measurements for each cell type. Metabolite flux values, with units of nmol/hr/25 million cells, were calculated for each metabolite peak in each cell type from the slope of their mass accumulation vs time plot. To determine the total ^{13}C-carbon flux for each metabolite peak the metabolite flux value for that peak was summed with any downstream metabolite flux value.

QUANTIFICATION AND STATISTICAL ANLAYSIS

One-way ANOVA was utilized to evaluate statistical significance of ECAR, OCR, qRT-PCR, ^{13}C metabolite measurements and enzyme activity assays. Statistical analysis was performed using Prism 7 (GraphPad). Unless otherwise noted n=3 for each experiment where n represents the number of independent replicates. For each experiment the specific statistical details can be found in the figure legends.

DATA AND SOFTWARE AVAILABILITY

The RNA-seq data for WA09 hESCs and DE, Meso, NPCs and NCSCs generated from WA09 hESCs have been deposited in the Gene Expression Omnibus under ID code GSE101655.

Supplementary Material

Refer to Web version on PubMed Central for supplementary material.

Acknowledgments

This work was supported by the National Institutes of Health, Institute of General Medical Sciences (P01GM085354) and benefitted from an upgrade to NMR under a shared instrumentation grant from the National Center for Research Resources, 1S10RR027097.

References

Adhikary S, Peukert K, Karsunky H, Beuger V, Lutz W, Elsässer H-P, Möröy T, Eilers M. Miz1 is required for early embryonic development during gastrulation. Molecular and Cellular Biology. 2003; 23:7648–7657. [PubMed: 14560010]

Berger RP, Sun YH, Kulik M, Lee JK, Nairn AV, Moremen KW, Pierce M, Dalton S. ST8SIA4-Dependent Polysialylation is Part of a Developmental Program Required for Germ Layer Formation from Human Pluripotent Stem Cells. Stem Cells. 2016; 34:1742–1752. [PubMed: 27074314]

Bergmeyer HU, Bernt E, Hess B. Lactate dehydrogenase. Methods of Enzymatic Analysis. 1974; 2:574–579.

Bernstein BE, Stamatoyannopoulos JA, Costello JF, Ren B, Milosavljevic A, Meissner A, Kellis M, Marra MA, Beaudet AL, Ecker JR, et al. The NIH Roadmap Epigenomics Mapping Consortium. Nat Biotechnol. 2010; 28:1045–1048. [PubMed: 20944595]

Blackwood E, Eisenman R. Max: a helix-loop-helix zipper protein that forms a sequence-specific DNA-binding complex with Myc. Science. 1991; 251:1211–1217. [PubMed: 2006410]

Candelario KM, Shuttleworth CW, Cunningham LA. Neural stem/progenitor cells display a low requirement for oxidative metabolism independent of hypoxia inducible factor-1alpha expression. J. Neurochem. 2013; 125:420–429. [PubMed: 23410250]

Cao Y, Guo WT, Tian S, He X, Wang XW, Liu X, Gu KL, Ma X, Huang D, Hu L, et al. miR-290/371-Mbd2-Myc circuit regulates glycolytic metabolism to promote pluripotency. The EMBO Journal. 2015; 34:609–623. [PubMed: 25603933]

Cartwright P, McLean C, Sheppard A, Rivett D, Jones K, Dalton S. LIF/STAT3 controls ES cell self-renewal and pluripotency by a Myc-dependent mechanism. Development. 2005; 132:885–896. [PubMed: 15673569]

Chambers SM, Fasano CA, Papapetrou EP, Tomishima M, Sadelain M, Studer L. Highly efficient neural conversion of human ES and iPS cells by dual inhibition of SMAD signaling. Nat Biotechnol. 2009; 27:275–280. [PubMed: 19252484]

Christofk HR, Vander Heiden MG, Harris MH, Ramanathan A, Gerszten RE, Wei R, Fleming MD, Schreiber SL, Cantley LC. The M2 splice isoform of pyruvate kinase is important for cancer metabolism and tumour growth. Nature. 2008; 452:230–233. [PubMed: 18337823]

Chu L-F, Leng N, Zhang J, Hou Z, Mamott D, Vereide DT, Choi J, Kendziorski C, Stewart R, Thomson JA. Single-cell RNA-seq reveals novel regulators of human embryonic stem cell differentiation to definitive endoderm. Genome Biol. 2016; 17:173. [PubMed: 27534536]

Cliff TS, Dalton S. Metabolic switching and cell fate decisions: implications for pluripotency, reprogramming and development. Curr. Opin. Genet. Dev. 2017; 46:44–49. [PubMed: 28662447]

Esen E, Chen J, Karner CM, Okunade AL, Patterson BW, Long F. WNT-LRP5 signaling induces Warburg effect through mTORC2 activation during osteoblast differentiation. Cell Metabolism. 2013; 17:745–755. [PubMed: 23623748]

Fantin VR, St-Pierre J, Leder P. Attenuation of LDH-A expression uncovers a link between glycolysis, mitochondrial physiology, and tumor maintenance. Cancer Cell. 2006; 9:425–434. [PubMed: 16766262]

Folmes CDL, Nelson TJ, Martinez-Fernandez A, Arrell DK, Lindor JZ, Dzeja PP, Ikeda Y, Perez-Terzic C, Terzic A. Somatic Oxidative Bioenergetics Transitions into Pluripotency-Dependent Glycolysis to Facilitate Nuclear Reprogramming. Cell Metabolism. 2011; 14:264–271. [PubMed: 21803296]

Golebiewska A, Atkinson SP, Lako M, Armstrong L. Epigenetic landscaping during hESC differentiation to neural cells. Stem Cells. 2009; 27:1298–1308. [PubMed: 19489095]

Gu W, Gaeta X, Sahakyan A, Chan AB, Hong CS, Kim R, Braas D, Plath K, Lowry WE, Christofk HR. Glycolytic Metabolism Plays a Functional Role in Regulating Human Pluripotent Stem Cell State. Cell Stem Cell. 2016; 19:476–490. [PubMed: 27618217]

Hsieh AL, Walton ZE, Altman BJ, Stine ZE, Dang CV. MYC and metabolism on the path to cancer. Semin. Cell Dev. Biol. 2015; 43:11–21. [PubMed: 26277543]

Jan C-I, Tsai M-H, Chiu C-F, Huang Y-P, Liu CJ, Chang NW. Fenofibrate Suppresses Oral Tumorigenesis via Reprogramming Metabolic Processes: Potential Drug Repurposing for Oral Cancer. Int. J. Biol. Sci. 2016; 12:786–798. [PubMed: 27313493]

Kerosuo L, Piltti K, Fox H, Angers-Loustau A, Häyry V, Eilers M, Sariola H, Wartiovaara K. Myc increases self-renewal in neural progenitor cells through Miz-1. Journal of Cell Science. 2008; 121:3941–3950. [PubMed: 19001505]

Kida YS, Kawamura T, Wei Z, Sogo T, Jacinto S, Shigeno A, Kushige H, Yoshihara E, Liddle C, Ecker JR, et al. ERRs Mediate a Metabolic Switch Required for Somatic Cell Reprogramming to Pluripotency. Cell Stem Cell. 2015; 16:547–555. [PubMed: 25865501]

Kim D, Pertea G, Trapnell C, Pimentel H, Kelley R, Salzberg SL. TopHat2: accurate alignment of transcriptomes in the presence of insertions, deletions and gene fusions. Genome Biol. 2013; 14:R36. [PubMed: 23618408]

Kim J, Woo AJ, Chu J, Snow JW, Fujiwara Y, Kim CG, Cantor AB, Orkin SH. A Myc network accounts for similarities between embryonic stem and cancer cell transcription programs. Cell. 2010; 143:313–324. [PubMed: 20946988]

Kirkeby A, Grealish S, Wolf DA, Nelander J, Wood J, Lundblad M, Lindvall O, Parmar M. Generation of regionally specified neural progenitors and functional neurons from human embryonic stem cells under defined conditions. Cell Reports. 2012; 1:703–714. [PubMed: 22813745]

Kriks S, Shim J-W, Piao J, Ganat YM, Wakeman DR, Xie Z, Carrillo-Reid L, Auyeung G, Antonacci C, Buch A, et al. Dopamine neurons derived from human ES cells efficiently engraft in animal models of Parkinson's disease. Nature. 2011; 480:547–551. [PubMed: 22056989]

Landor SK-J, Mutvei AP, Mamaeva V, Jin S, Busk M, Borra R, Grönroos TJ, Kronqvist P, Lendahl U, Sahlgren CM. Hypo- and hyperactivated Notch signaling induce a glycolytic switch through distinct mechanisms. Proceedings of the National Academy of Sciences. 2011; 108:18814–18819.

Lin C-H, Lin C, Tanaka H, Fero ML, Eisenman RN. Gene regulation and epigenetic remodeling in murine embryonic stem cells by c-Myc. PLoS ONE. 2009; 4:e7839. [PubMed: 19915707]

Lopaschuk GD, Jaswal JS. Energy metabolic phenotype of the cardiomyocyte during development, differentiation, and postnatal maturation. J. Cardiovasc. Pharmacol. 2010; 56:130–140. [PubMed: 20505524]

Malynn BA, de Alboran IM, O'Hagan RC, Bronson R, Davidson L, DePinho RA, Alt FW. N-myc can functionally replace c-myc in murine development, cellular growth, and differentiation. Genes & Development. 2000; 14:1390–1399. [PubMed: 10837031]

McCarthy DJ, Chen Y, Smyth GK. Differential expression analysis of multifactor RNA-Seq experiments with respect to biological variation. Nucleic Acids Research. 2012; 40:4288–4297. [PubMed: 22287627]

Menendez L, Kulik MJ, Page AT, Park SS, Lauderdale JD, Cunningham ML, Dalton S. Directed differentiation of human pluripotent cells to neural crest stem cells. Nat Protoc. 2013; 8:203–212. [PubMed: 23288320]

Miccheli A, Tomassini A, Puccetti C, Valerio M, Peluso G, Tuccillo F, Calvani M, Manetti C, Conti F. Metabolic profiling by 13C–NMR spectroscopy: [1,2-13C2]glucose reveals a heterogeneous metabolism in human leukemia T cells. Biochimie. 2006; 88:437–448. [PubMed: 16359766]

Moussaieff A, Kogan NM, Aberdam D. Concise Review: Energy Metabolites: Key Mediators of the Epigenetic State of Pluripotency. Stem Cells. 2015a; 33:2374–2380. [PubMed: 25873344]

Moussaieff A, Rouleau M, Kitsberg D, Cohen M, Levy G, Barasch D, Nemirovski A, Shen-Orr S, Laevsky I, Amit M, et al. Glycolysis-Mediated Changes in Acetyl-CoA and Histone Acetylation Control the Early Differentiation of Embryonic Stem Cells. Cell Metabolism. 2015b; 21:392–402. [PubMed: 25738455]

Myers SA, Peddada S, Chatterjee N, Friedrich T, Tomoda K, Krings G, Thomas S, Maynard J, Broeker M, Thomson M, et al. SOX2 O-GlcNAcylation alters its protein-protein interactions and genomic occupancy to modulate gene expression in pluripotent cells. Elife. 2016; 5:e10647. [PubMed: 26949256]

Patra KC, Wang Q, Bhaskar PT, Miller L, Wang Z, Wheaton W, Chandel N, Laakso M, Muller WJ, Allen EL, et al. Hexokinase 2 is required for tumor initiation and maintenance and its systemic deletion is therapeutic in mouse models of cancer. Cancer Cell. 2013; 24:213–228. [PubMed: 23911236]

Qiao Y, Wang R, Yang X, Tang K, Jing N. Dual Roles of Histone H3 Lysine 9 Acetylation in Human Embryonic Stem Cell Pluripotency and Neural Differentiation. Journal of Biological Chemistry. 2015; 290:2508–2520. [PubMed: 25519907]

Ritchie ME, Phipson B, Wu D, Hu Y, Law CW, Shi W, Smyth GK. limma powers differential expression analyses for RNA-sequencing and microarray studies. Nucleic Acids Research. 2015; 43:e47. [PubMed: 25605792]

Robinson MD, McCarthy DJ, Smyth GK. edgeR: a Bioconductor package for differential expression analysis of digital gene expression data. Bioinformatics. 2010; 26:139–140. [PubMed: 19910308]

Ryall JG, Cliff T, Dalton S, Sartorelli V. Metabolic Reprogramming of Stem Cell Epigenetics. Cell Stem Cell. 2015a; 17:651–662. [PubMed: 26637942]

Ryall JG, Dell'Orso S, Derfoul A, Juan A, Zare H, Feng X, Clermont D, Koulnis M, Gutierrez-Cruz G, Fulco M, et al. The NAD(+)-dependent SIRT1 deacetylase translates a metabolic switch into regulatory epigenetics in skeletal muscle stem cells. Cell Stem Cell. 2015b; 16:171–183. [PubMed: 25600643]

Schneider CA, Rasband WS, Eliceiri KW. NIH Image to ImageJ: 25 years of image analysis. Nat Chem Biol. 2012; 9:671–675.

Sekine N, Cirulli V, Regazzi R, Brown LJ, Gine E, Tamarit-Rodriguez J, Girotti M, Marie S, MacDonald MJ, Wollheim CB. Low lactate dehydrogenase and high mitochondrial glycerol phosphate dehydrogenase in pancreatic beta-cells. Potential role in nutrient sensing. J Biol Chem. 1994; 269:4895–4902. [PubMed: 8106462]

Shiraki N, Shiraki Y, Tsuyama T, Obata F, Miura M, Nagae G, Aburatani H, Kume K, Endo F, Kume S. Methionine metabolism regulates maintenance and differentiation of human pluripotent stem cells. Cell Metabolism. 2014; 19:780–794. [PubMed: 24746804]

Shyh-Chang N, Daley GQ. Metabolic Switches Linked to Pluripotency and Embryonic Stem Cell Differentiation. Cell Metabolism. 2015; 21:349–350. [PubMed: 25738450]

Si-Tayeb K, Noto FK, Sepac A, Sedlic F, Bosnjak ZJ, Lough JW, Duncan SA. Generation of human induced pluripotent stem cells by simple transient transfection of plasmid DNA encoding reprogramming factors. BMC Dev. Biol. 2010; 10:81. [PubMed: 20682060]

Singh AM, Sun Y, Li L, Zhang W, Wu T, Zhao S, Qin Z, Dalton S. Cell-Cycle Control of Bivalent Epigenetic Domains Regulates the Exit from Pluripotency. Stem Cell Reports. 2015; 5:323–336. [PubMed: 26278042]

Smith KN, Singh AM, Dalton S. Myc Represses Primitive Endoderm Differentiation in Pluripotent Stem Cells. Cell Stem Cell. 2010; 7:343–354. [PubMed: 20804970]

Stine ZE, Walton ZE, Altman BJ, Hsieh AL, Dang CV. MYC, Metabolism, and Cancer. Cancer Discov. 2015; 5:1024–1039. [PubMed: 26382145]

Su S, Law CW, Ah-Cann C, Asselin-Labat M-L, Blewitt ME, Ritchie ME. Glimma: interactive graphics for gene expression analysis. Bioinformatics. 2017; 33:2050–2052. [PubMed: 28203714]

Teperino R, Amann S, Bayer M, McGee SL, Loipetzberger A, Connor T, Jaeger C, Kammerer B, Winter L, Wiche G, et al. Hedgehog partial agonism drives Warburg-like metabolism in muscle and brown fat. Cell. 2012; 151:414–426. [PubMed: 23063129]

Trapnell C, Roberts A, Goff L, Pertea G, Kim D, Kelley DR, Pimentel H, Salzberg SL, Rinn JL, Pachter L. Differential gene and transcript expression analysis of RNA-seq experiments with TopHat and Cufflinks. Nat Protoc. 2012; 7:562–578. [PubMed: 22383036]

Tsankov AM, Gu H, Akopian V, Ziller MJ, Donaghey J, Amit I, Gnirke A, Meissner A. Transcription factor binding dynamics during human ES cell differentiation. Nature. 2015; 518:344–349. [PubMed: 25693565]

Ulrich EL, Akutsu H, Doreleijers JF, Harano Y, Ioannidis YE, Lin J, Livny M, Mading S, Maziuk D, Miller Z, et al. BioMagResBank. Nucleic Acids Research. 2008; 36:D402–D408. [PubMed: 17984079]

van de Leemput J, Boles NC, Kiehl TR, Corneo B, Lederman P, Menon V, Lee C, Martinez RA, Levi BP, Thompson CL, et al. CORTECON: a temporal transcriptome analysis of in vitro human cerebral cortex development from human embryonic stem cells. Neuron. 2014; 83:51–68. [PubMed: 24991954]

Vander Heiden MG, Cantley LC, Thompson CB. Understanding the Warburg effect: the metabolic requirements of cell proliferation. Science. 2009; 324:1029–1033. [PubMed: 19460998]

Varlakhanova NV, Cotterman RF, deVries WN, Morgan J, Donahue LR, Murray S, Knowles BB, Knoepfler PS. Myc maintains embryonic stem cell pluripotency and self-renewal. Differentiation. 2010; 80:9–19. [PubMed: 20537458]

Varum S, Rodrigues AS, Moura MB, Momcilovic O, Easley CA, Ramalho-Santos J, Van Houten B, Schatten G. Energy metabolism in human pluripotent stem cells and their differentiated counterparts. PLoS ONE. 2011; 6:e20914. [PubMed: 21698063]

Wang YY, Attané C, Milhas D, Dirat B, Dauvillier S, Guerard A, Gilhodes J, Lazar I, Alet N, Laurent V, et al. Mammary adipocytes stimulate breast cancer invasion through metabolic remodeling of tumor cells. JCI Insight. 2017; 2:e87489. [PubMed: 28239646]

Wishart DS, Jewison T, Guo AC, Wilson M, Knox C, Liu Y, Djoumbou Y, Mandal R, Aziat F, Dong E, et al. HMDB 3.0--The Human Metabolome Database in 2013. Nucleic Acids Research. 2013; 41:D801–D807. [PubMed: 23161693]

Yang Y-L, Li J, Liu K, Zhang L, Liu Q, Liu B, Qi L-W. Ginsenoside Rg5 increases cardiomyocyte resistance to ischemic injury through regulation of mitochondrial hexokinase-II and dynamin-related protein 1. Cell Death Dis. 2017; 8:e2625. [PubMed: 28230856]

Zhang J, Khvorostov I, Hong JS, Oktay Y, Vergnes L, Nuebel E, Wahjudi PN, Setoguchi K, Wang G, Do A, et al. UCP2 regulates energy metabolism and differentiation potential of human pluripotent stem cells. The EMBO Journal. 2011; 30:4860–4873. [PubMed: 22085932]

Zheng X, Boyer L, Jin M, Mertens J, Kim Y, Ma L, Ma L, Hamm M, Gage FH, Hunter T. Metabolic reprogramming during neuronal differentiation from aerobic glycolysis to neuronal oxidative phosphorylation. Elife. 2016; 5

Zhou W, Choi M, Margineantu D, Margaretha L, Hesson J, Cavanaugh C, Blau CA, Horwitz MS, Hockenbery D, Ware C, et al. HIF1a induced switch from bivalent to exclusively glycolytic metabolism during ESC-to-EpiSC/hESC transition. The EMBO Journal. 2012; 31:2103–2116. [PubMed: 22446391]

Highlights

- Metabolic switching during hPSC differentiation is germ layer-specific
- Switching is restricted to mesoderm and endoderm following exit from pluripotency
- Early ectodermal differentiation requires maintenance of high glycolytic flux
- Switching is controlled by MYC/MYCN and couples metabolism to cell fate decisions

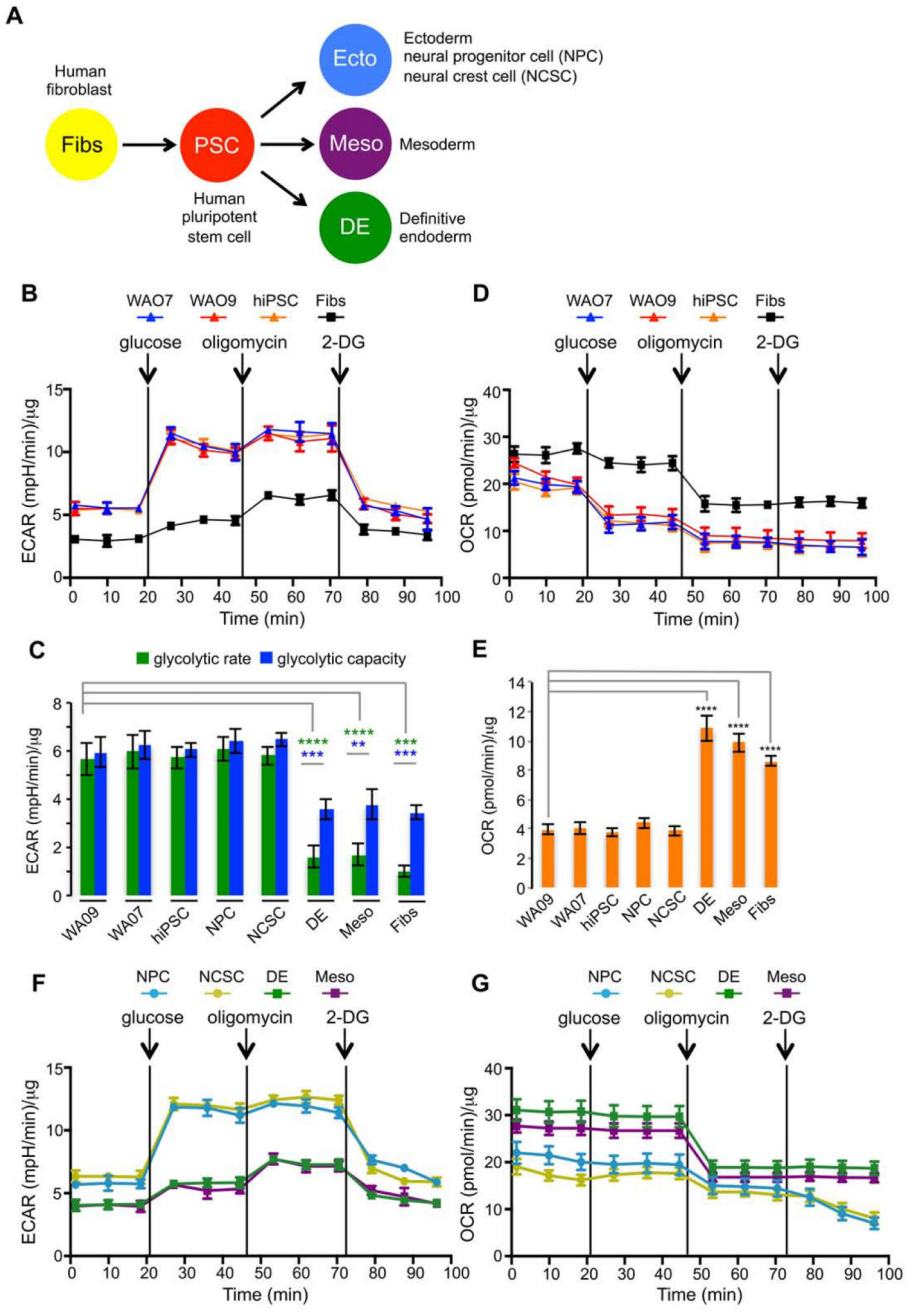

Figure 1. Metabolic switching as cells exit pluripotency is germ layer-specific

(**A**) Summary of cell types used in this study. (**B**) Extracellular acidification rate (ECAR) analysis of human pluripotent stem cells (hESCs; WA07, WA09, hiPSCs) and primary human fibroblasts (Fibs) following addition of glucose (10 mM), oligomycin (1 mM) and 2-deoxyglucose (2-DG, 50 mM). (**C**) Glycolytic rates (ECAR) and glycolytic capacity (ECAR following oligomycin) for hPSCs, Fibs, neural progenitor cells (NPC), pre-neural crest stem cells (NCSC), definitive endoderm (DE) and mesoderm (Meso). (**D**) Oxygen consumption rate (OCR) assays for hPSCs and Fibs. (**E**) OCRs for the indicated cell types. (**F,G**) ECAR and OCR analysis for the indicated cell types. All assays were performed in biological

triplicate. Error bars represent the standard deviation. **** $p<0.0001$, *** $p<0.001$, ** $p<0.01$ for Students pair-wise t-test. See also Figure S1. Note: non-statically significant changes are not denoted on graphs; only significant changes are labeled.

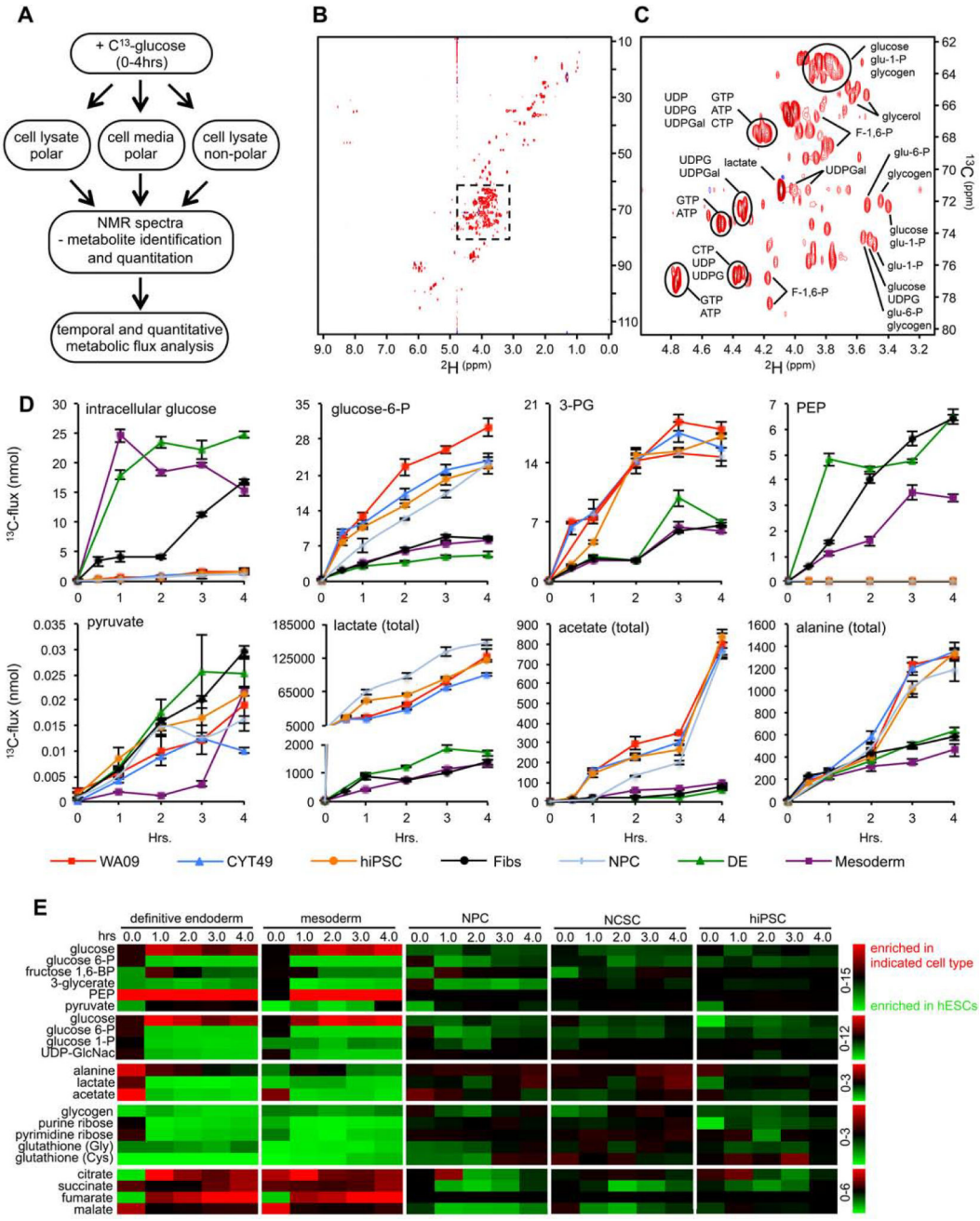

Figure 2. Nuclear magnetic resonance (NMR) analysis of metabolic switching

(**A**) Workflow for NMR-based ^{13}C-glucose metabolic flux analysis. (**B**) Representative gradient enhanced 1D-^{1}H and 2D-^{1}H, ^{13}C-heteronuclear single quantum coherence (cCHSQC) NMR spectra (Figures 2B–C). Each peak measures an individual carbon to hydrogen bond within metabolites that can be identified and quantitated. (**C**) Magnification of NMR spectra shown in boxed area of (B). Representative metabolites are indicated. (**D**)^{13}C-flux analysis over a 0–4 hr time-course for definitive endoderm (DE), mesoderm (Meso), neural progenitor cells (NPC), pre-neural crest stem cells (NCSC) and hiPSCs. Measurements are of intracellular metabolites unless observed in both the intra- and

extracellular fractions and are then marked by (total), which represents the combination of intra- and extra-cellular measurements. Scale bars are shown (right). (**E**) NMR-based ^{13}C-glucose metabolic flux analysis over a 4 hr labeling time-course for indicated metabolites in glycolysis, hexosamine biosynthetic pathway, the pentose phosphate pathway, glycogen biosynthesis, glutathione production and the tricarboxylic acid cycle within pluripotent cells (WA09, Cyt49, hiPSC), WA09-derived germ layer derivatives (NPC, DE, Meso) and primary fibroblasts (Fibs). Metabolite levels for indicated cell types are displayed as the fold-change to metabolite levels at corresponding time points in hESCs (WA09). See also Figure S2.

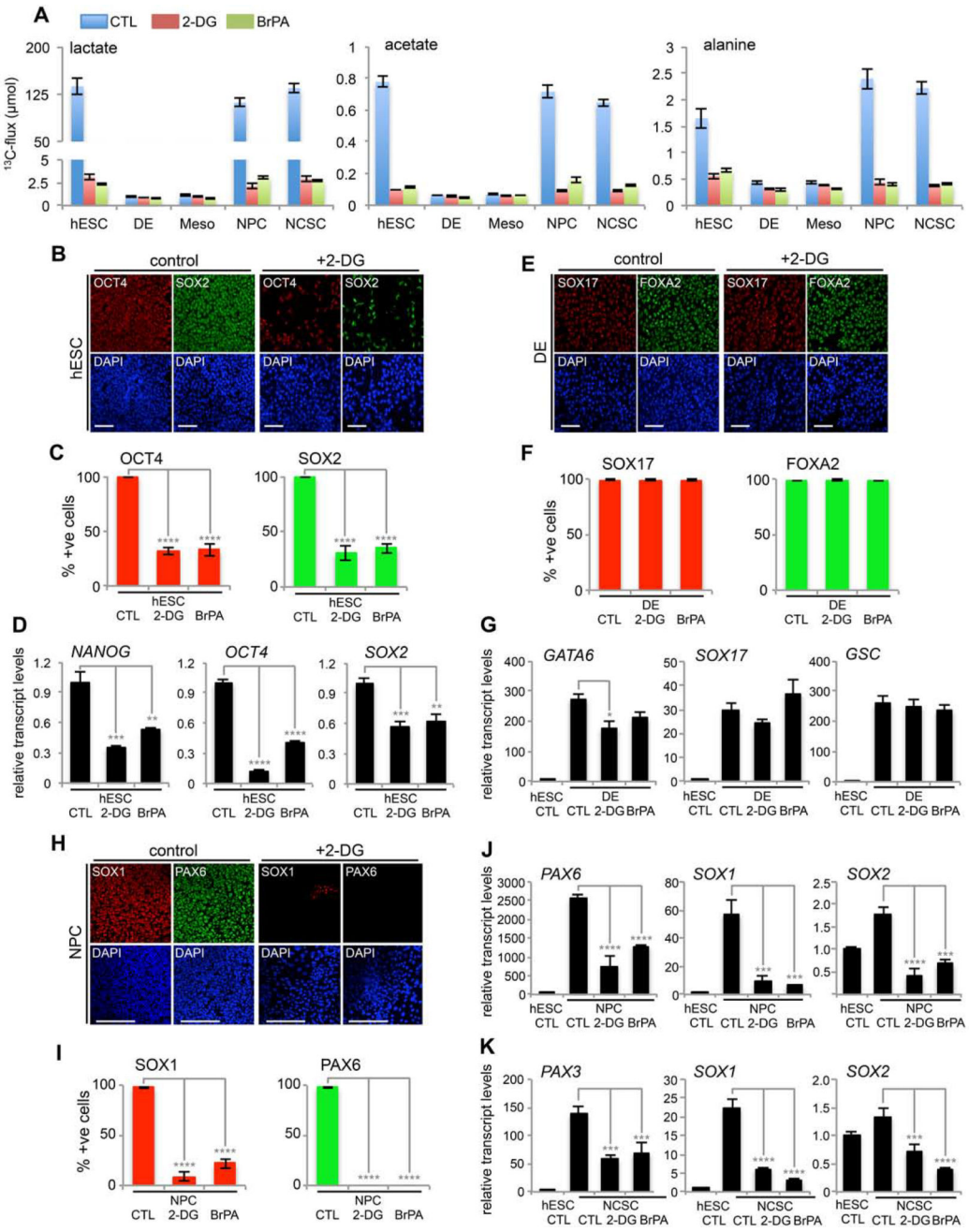

Figure 3. Elevated glycolytic activity is required for pluripotency and early ectoderm differentiation

(**A**) ^{13}C-glucose metabolic flux analysis over 4 hr in hESCs, definitive endoderm (DE), mesoderm (Meso) and early ectoderm- neural progenitor cells (NPCs) and pre-neural crest stem cells (NCSC). 24 hours after plating, cells were cultured for a further 3 days (hESCs, DE and Meso) or 5 days (NPC and NCSC) in the presence of 2-deoxyglucose (2-DG, 2.2 mM) or 3-bromopyruvate (BrPA, 17µM) where indicated. Units are nmol standardized to 25 million cells. Error bars represent the standard deviation. Cells were immunostained and probed for indicated antibodies, then scored for % cells expressing lineage markers (red and green bar graphs) and analyzed by qRT-PCR (black bar graphs) analysis to determine

transcript levels in WA09 hESCs (**B–D**), DE (**E–G**) or NPCs (**H–J**). (**K**) qRT-PCR transcript analysis of *PAX3*, *SOX1* and *SOX2* in hESCs and NCSC that were seeded and cultured for 24 hrs, then treated with 2-DG (2.2 mM) or BrPA (17 μM), as indicated for 5 days. **** $p<0.0001$, *** $p<0.001$, ** $p<0.01$ for one-way ANOVA. All experiments were performed in biological triplicate. Error bars represent the standard deviation. Micron bars, 100 mm. See also Figure S3, S4 and S5.

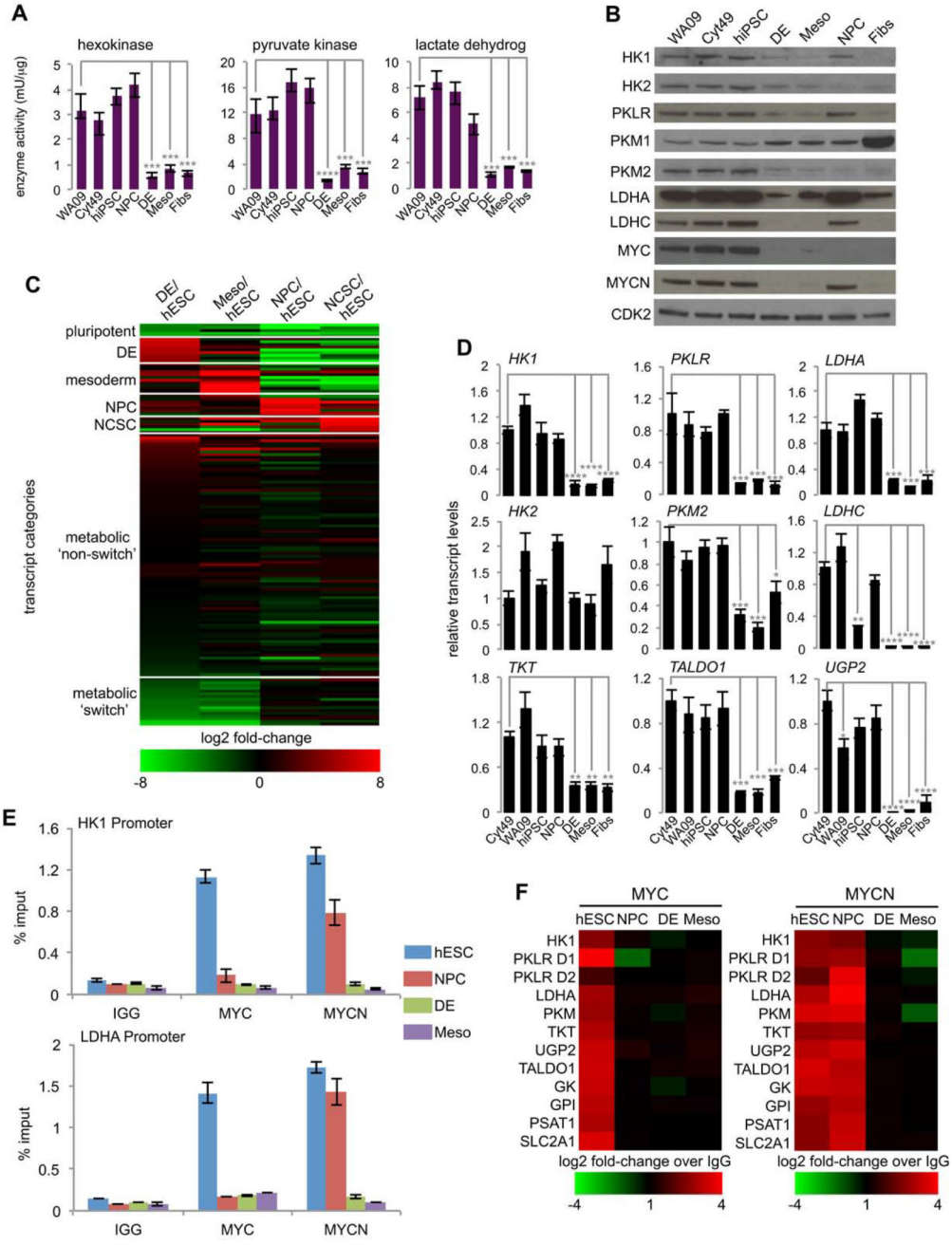

Figure 4. Metabolic switch genes are MYC/MYCN targets

(**A**) Enzyme activities assayed in cell lysates from the indicated cell types. (**B**) Immunoblot analysis of hPSC (WA09, Cyt49, hiPSC), definitive endoderm (DE), mesoderm (Meso), ectoderm (NPC; neural progenitor cell) and primary human fibroblast (Fibs) cell lysates probed with the indicated antibodies. (**C**) RNA-seq analysis of cell identity and metabolic genes in hESCs compared to derivative cell types; DE, Meso and ectoderm (NPC and pre-neural crest stem cells; NCSC). Metabolic 'non-switch' and 'switch' transcripts are indicated as are cell identity genes for each cell type (see Table S1). (**D**) qRT-PCR analysis of representative metabolic 'switch' transcripts in hPSCs, NPC, Meso, DE and Fibs. (**E**)

Quantitative ChIP assays of MYC and MYCN binding to the promoters of HK1 and LDHA in hESCs and the three germ layers with immunoglobulin G (IgG) as the control. (**F**) Heat map of quantitative ChIP assays showing binding of MYC and MYCN as the log2 fold change over IgG control to metabolic 'switch' genes in hESCs and the three germ layers. **** $p<0.0001$, *** $p<0.001$, ** $p<0.01$ for one-way ANOVA. All experiments were performed in biological triplicate. Error bars represent the standard deviation. See also Table S1.

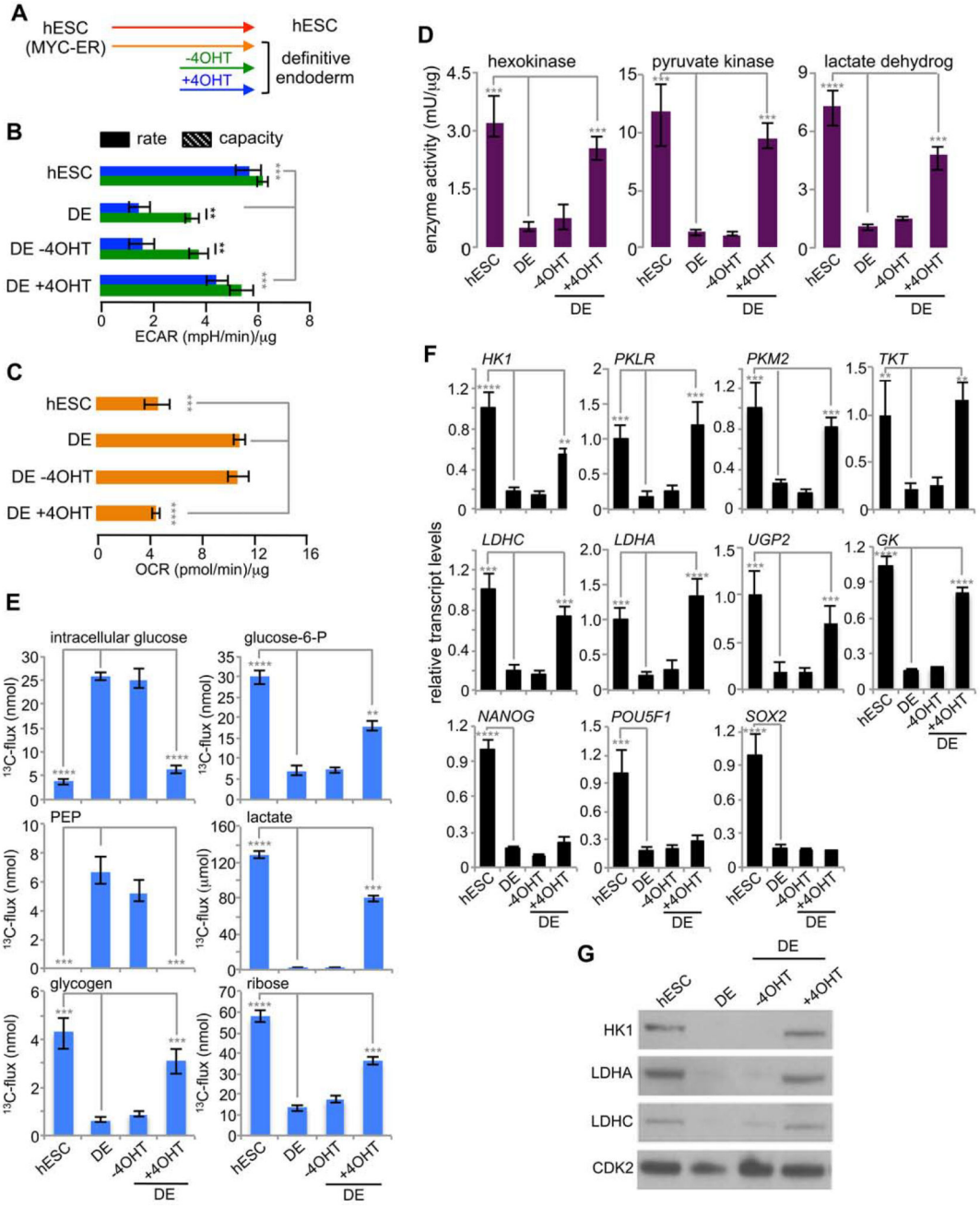

Figure 5. MYC is sufficient to re-establish the pluripotent mode of metabolic activity in endodermal cells

(**A**) Experimental scheme where a MYC-ER transgene is under control of 4OHT. (**B**) Extracellular acidification rate (ECAR) measurements in WA09 hESCs, derivative definitive endoderm (DE) and DE from hESCs carrying a MYC-ER transgene (+/− 4OHT) final 48 hours of differentiation. Oxygen consumption rate (OCR) analysis (**C**), enzyme activity assays (**D**) ^{13}C-glucose metabolic flux analysis over 4 hr (**E**), qRT-PCR (**F**) and immunoblot analysis (**G**) under conditions described in (B). **** p<0.0001, *** p<0.001, ** p<0.01 for

one-way ANOVA. All experiments were performed in biological triplicate. Error bars represent the standard deviation. See also Figure S6.

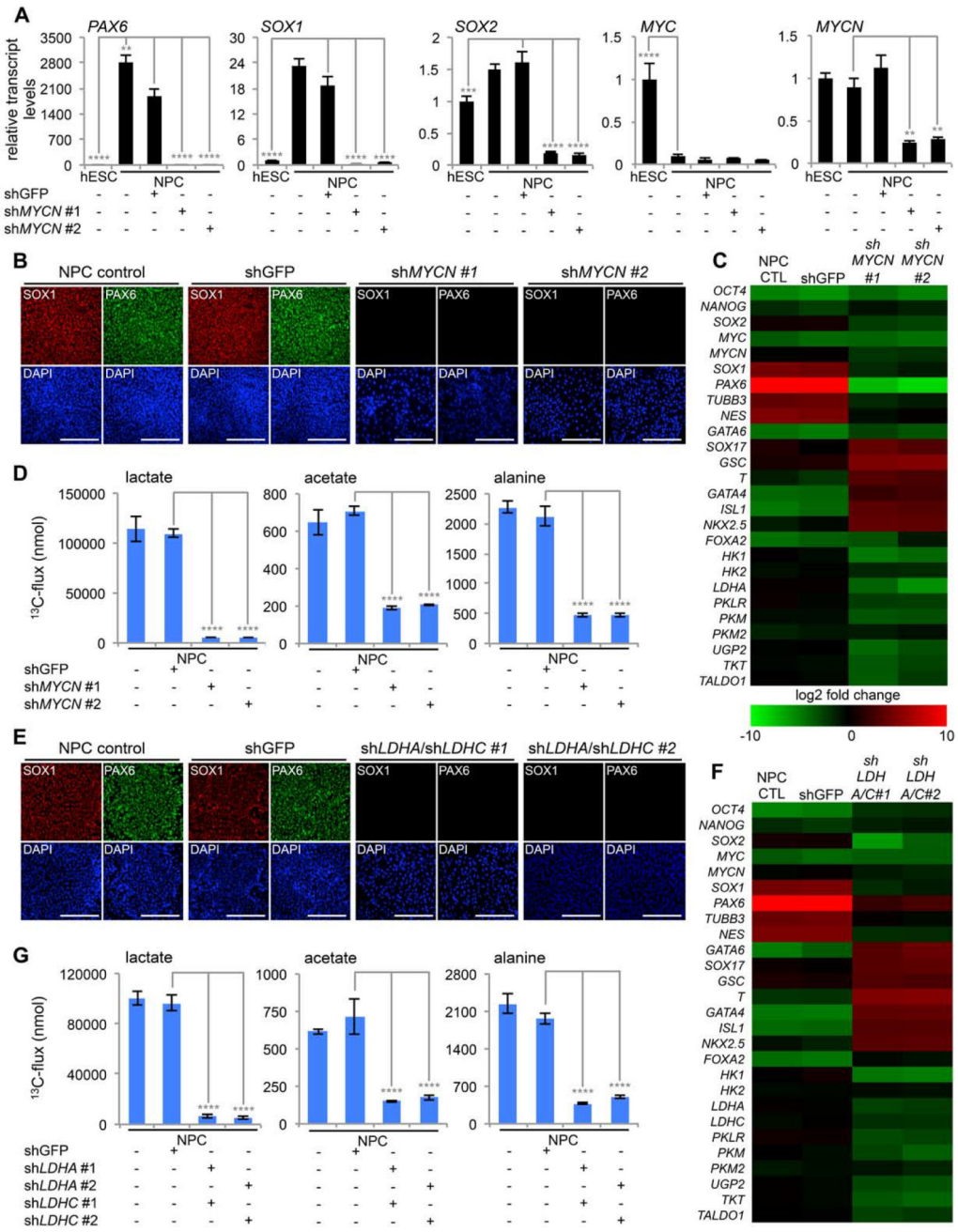

Figure 6. MYC activity is required for maintenance of metabolic flux in pluripotent cells and during the early ectoderm transition

(**A**) qRT-PCR transcript analysis of WA09 hESCs, WA09-derived NPCs and NPCs transduced with lentivirus expressing GFP shRNA, *MYCN* shRNA#1, or *MYCN* shRNA#2. (**B**) Immunofluorescence showing levels of differentiation marker expression in control, GFP shRNA, *MYCN* shRNA#1, or *MYCN* shRNA#2 lentivirus transduced NPCs. qRT-PCR heat map of pluripotency and differentiation marker transcripts and metabolic 'switch' transcripts (**C**) and ^{13}C-glucose metabolic flux analysis (**D**) of NPCs transduced with GFP shRNA, *MYCN* shRNA#1, or *MYCN* shRNA#2 lentivirus for 5 days. (**E**)

Immunofluorescence showing levels of differentiation marker expression in WA09-derived control NPCs, NPCs transduced with lentivirus expressing GFP shRNA, co-expressing *LDHA* shRNA#1 and *LDHC* shRNA#1, or co-expressing *LDHA* shRNA#2 and *LDHC* shRNA#2. qRT-PCR heat map of pluripotency and differentiation marker transcripts and metabolic 'switch' transcripts (**F**) and ^{13}C-glucose metabolic flux analysis (**G**) of NPCs transduced with lentivirus expressing GFP shRNA, co-expressing *LDHA* shRNA#1 and *LDHC* shRNA#1, or co-expressing *LDHA* shRNA#2 and *LDHC* shRNA#2 for 5 days. **** $p<0.0001$, *** $p<0.001$, ** $p<0.01$ for one-way ANOVA. All experiments were performed in biological triplicate. Error bars represent the standard deviation. Micron bars, 100 mm. See also Figure S7.

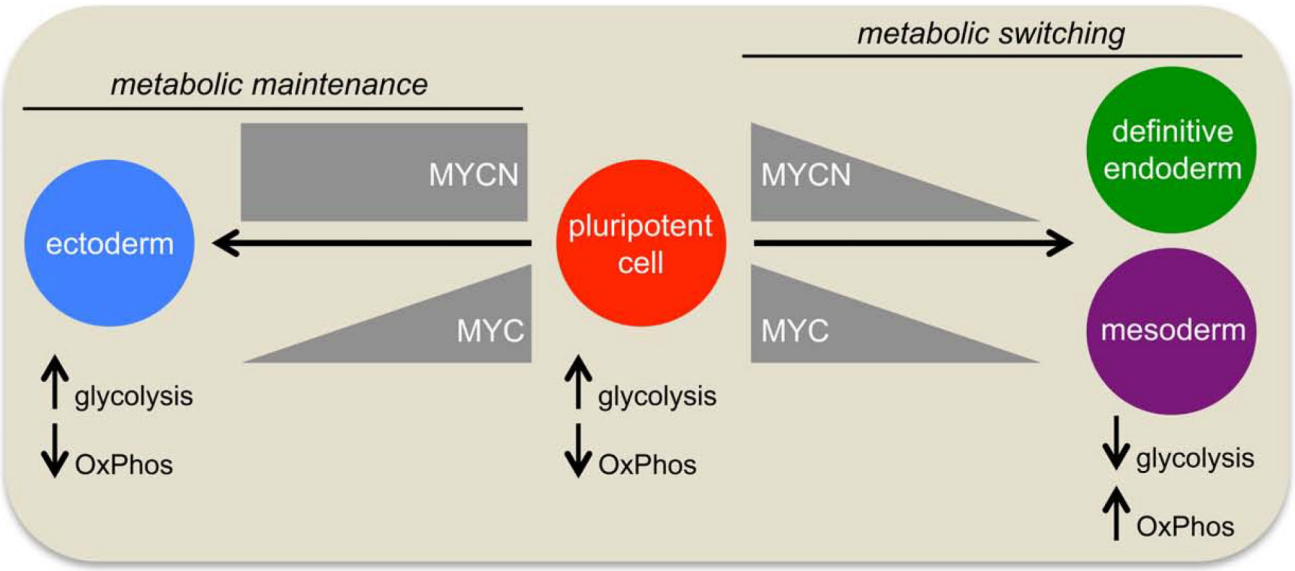

Figure 7. Mechanism by which MYC couples cell fate decisions to metabolic activity

MYC and MYCN maintain high glycolytic flux and pluripotency of human pluripotent cells by maintaining the transcriptional activity of metabolic 'switch' genes. During differentiation to definitive endoderm and mesoderm, global MYC levels decrease, metabolic 'switch' genes are down-regulated and glycolytic flux decreases. During early ectoderm commitment, MYC levels decline but MYCN activity is maintained- this maintains the transcription of metabolic 'switch' genes and an elevated glycolytic flux that is required for the pluripotency to ectoderm transition.